Contents

Global Climate Models and 20th and 21st Century Arctic Climate Change

Cecilia M. Bitz[1], Jeff K. Ridley[2], Marika Holland[3], and Howard Cattle[4]

[1] Atmospheric Sciences, University of Washington, Seattle, WA, USA
bitz@atmos.washington.edu
[2] Hadley Centre for Climate Prediction, Met Office, Exeter, UK
jeff.ridley@metoffice.gov.uk
[3] National Center for Atmospheric Research, Boulder, CO, USA
mholland@ucar.edu
[4] National Oceanography Centre, Southampton, UK hyc@noc.soton.ac.uk

Abstract

We review the history of global climate model (GCM) development with regard to Arctic climate beginning with the ACSYS era. This was a time of rapid improvement in many models. We focus on those aspects of the Arctic climate system that are most likely to amplify the Arctic response to anthropogenic greenhouse gas forcing in the 20th and 21st centuries. Lessons from past GCM modeling and the most likely near-future model developments are discussed. We present highlights of GCM simulations from two sophsiticated climate models that have the highest Arctic amplification among the the models that participated in the World Climate Research Programme's third Coupled Model Intercomparison Project (CMIP3). The two models are the Hadley Center Global Environmental Model (HadGEM1) and the Community Climate System Model version 3 (CCSM3). These two models have considerably larger climate change in the Arctic than the CMIP3 model mean by mid 21st century. Thus the surface warms by about 50% more on average north of 75°N in HadGEM1 and CCSM3 than in the CMIP3 model mean, which amounts to more than three times the global average warming. The sea ice thins and retreats 50-100% more in HadGEM1 and CCSM3 than in the CMIP3 model mean. Further, the oceanic transport of heat into the Arctic increases much more in HadGEM1 and CCSM3 than in other CMIP3 models and contributes to the larger climate change.

1 Introduction

The ACSYS era spanned a period of rapid developments in global climate models (GCMs), especially with regard to polar climates. In 1992 experiments

from only four global atmosphere-ocean general circulation models appeared in the Intergovernmental Panel on Climate Change supplementary assessment report (*IPCC*, 1992), while more than 20 different models provided their output for intercomparison in the most recent IPCC report (IPCC, 2007). Models in the earlier IPCC were coarse-resolution, had relatively simple physics, and the majority needed unphysical adjustments to the heat and moisture exchange between the ocean and atmosphere.

Before the ACSYS era, new physics developed for GCMs were usually designed and tested for midlatitude and tropical climate applications. The focus steered clear of the polar regions probably because most modelers thought that too little was known about polar processes and data were scarce (*Randall et al.*, 1998). Programs like ACSYS have helped expand our knowledge and observations of Arctic climate processes, so that GCM developers now pay special attention to the polar regions and high-latitude model physics are improving.

While early climate model development had little emphasis on high-latitude processes, Arctic climate simulated by the models has long attracted scientific attention. Even the earliest coupled atmosphere-ocean energy-balance models had an amplified response at the poles when subject to an increase in radiative forcing (*Budyko*, 1969; *Sellers*, 1969). Predictions in the early 1990s of future Arctic climate change were so dire that one of two questions in the ACSYS mission (see http://acsys.npolar.no) read, "Is the Arctic climate system as sensitive to increased greenhouse gas concentrations as climate models suggest?" But when comparing models and observations for the last two decades of the 20th century, studies find that the multi-model ensemble mean of the most current models agrees well with observed trends in Arctic surface air temperature and sea ice extent (*Arzel et al.*, 2006; *Zhang and Walsh*, 2006; *Wang et al.*, 2007). Now, after repeated record-setting sea ice conditions in recent decades, the question has turned full circle, and studies are asking if models can keep pace with observed trends (e.g., *Stroeve et al.*, 2007).

In this chapter, we describe some of the key GCM developments with regard to Arctic climate since the start of the ACSYS era (Section 2). We focus on those aspects of the Arctic climate system that are likely the most influential at amplifying the Arctic response to anthropogenic greenhouse gas forcing in the 20th and 21st centuries, including the sea ice component, ocean-atmosphere exchange and ocean mixing, and clouds. Next we present highlights of GCM simulations of the late 20th century climate and changes at mid 21st century from two models with the highest Arctic amplification of surface warming and compare them to the multi-model ensemble mean from the models that participated in the most recent World Climate Research Programme (WCRP) Coupled Model Intercomparison Project, which is version 3 (CMIP3) (*Meehl et al.*, 2007) (Section 3). These same models were analyzed for the IPCC fourth assessment report. A summary and future outlook are given at the end (Section 4).

2 GCM developments since the beginning of the ACSYS era

2.1 Sea Ice Component

Prior to the ACSYS era, sea ice in GCMs was treated as a slab of a single thickness that uniformly covered a grid box (e.g., sea ice could not co-exist with an ice-free fraction). Usually any snow that fell on top of sea ice was converted immediately to an equivalent sea ice thickness. Therefore the thermal insulating capacity of snow was neglected and the surface albedo did not depend explicitly on snow properties. Heat conduction through the sea ice was calculated by assuming a linear temperature profile between the top and bottom surfaces of the ice (as in the Semtner 1976 zero-layer sea ice model); hence, sea ice had zero heat capacity and surface temperature changes lead to no change in stored sensible heat. Surface albedo was highly parameterized to artificially account for leads, snow cover, and melt ponds, usually by varying with surface temperature and ice thickness. If the sea ice moved at all, it was advected with the surface currents — in what is known as "free drift". Once the sea ice thickness reached some threshold (4 m was common) it was then held motionless to prevent the sea ice from building to excess in regions of convergence. Early GCMs that employed such sea ice models are described in *Washington and Meehl* (1989), *Manabe et al.* (1991), and *McFarlane et al.* (1992).

It is now well known that sea ice dynamics has a first-order influence on the sea ice mean state, variability and sensitivity to radiative forcing. *Hibler* (1980) showed that a motionless sea ice model would have the thickest ice cover centered on the north pole, while a model with dynamics is needed to simulate the observed thick ice against Greenland and the Canadian Archipelago coasts. Additional studies with uncoupled, sea ice-only models indicated that adding sea ice dynamics to a sea ice component in a GCM would likely reduce the model's sensitivity to radiative forcing (*Hibler*, 1984; *Lemke et al.*, 1990; *Holland et al.*, 1993; *Fichefet and Morales Maqueda*, 1997). The results suggest that sea ice dynamics acts as a negative feedback on sea ice thickness because thinner ice more easily converges and deforms (building thickness dynamically and increasing winter open water formation and ice growth rates), while thicker ice resists dynamical thickening. The association of sea ice dynamics with negative feedback was verified in at least three separate GCMs where studies showed models with dynamics tend to retreat less in response to increasing radiative forcing than the same model with sea ice held motionless (*Vavrus*, 1999; *Holland et al.*, 2001; *Hewitt et al.*, 2001; *Vavrus and Harrison*, 2003).

Several of the first GCMs to include sea ice dynamics adopted the cavitating fluid (CF) sea ice dynamics from *Flato and Hibler* (1992) (e.g., the early NCAR and CSIRO models, see Pollard and Thompson 1994 and Gordon and O'Farrel, 1997) because it offered simplicity and numerical efficiency

to describe the ice internal stress over the more comprehensive viscous-plastic (VP) rheology (*Hibler*, 1979). The VP rheology takes into account failure under compression and shear, while the CF physics disregard the influence of shear stress. Both VP and CF treatments assume the amalgam of sea ice floes and leads can be treated as a continuum. The first GCMs to employ the full VP physics were the ECHAM4+OPYC3 model (*Oberhuber*, 1993) and the ECHAM4+HOPE-G (ECHO-G) model (*Wolff et al.*, 1997). Among the models that participated in the first Coupled Model Intercomparison Project (CMIP1, see Meehl et al., 2000), which are contemporaries of these early GCMs with sea ice dynamics, 11 of 18 models had motionless sea ice and another 3 had ice in free drift. The first Sea Ice Model Intercomparison Project (SIMIP1), sponsored by ACSYS, took place roughly at the same time as CMIP1 and compared sea ice models with different dynamics schemes (*Lemke et al.*, 1997). SIMIP1 investigators found that the VP rheology produced a more realistic simulation than CF or free-drift models (*Kreyscher et al.*, 2000). In addition, they noted that the computational cost for the VP scheme was marginal compared to the rest of a typical GCM. A more efficient numerical scheme for ice rheology that could be adapted to parallel computing known as the elastic-viscous plastic (EVP) soon became available and made sea ice dynamics schemes even more attractive for GCMs (*Hunke and Dukowicz*, 1997; *Hunke and Zhang*, 2000; *Zhang and Rothrock*, 2000). Over half of the CMIP3 models, the most recent coupled model intercomparison project, have VP or EVP sea ice dynamics.

Sea ice thermodynamics still varies widely across sea ice components of global climate models. An effort to improve model thermodynamics ushered in the second Sea Ice Model Intercomparison Project (SIMIP2), which was a joint initiative of the ACSYS/CliC Numerical Experimentation Group and the GEWEX Cloud System Study, Working Group on Polar Clouds. One study from this project showed that a multi-layer sea ice model that explicitly resolved brine pockets reproduced well the sea ice thickness and temperature measured during the Surface Heat Budget of the Arctic Ocean (SHEBA) experiment (*Huwald et al.*, 2005). Global sea ice models have also shown how sea ice thermodynamics influences the mass, heat, and freshwater balance of the climate system. One-dimensional (*Maykut and Untersteiner*, 1971; *Semtner*, 1976) and global-scale (*Holland et al.*, 1993; *Fichefet and Morales Maqueda*, 1997; *Bitz et al.*, 2001) models showed that taking into account internal melt in brine pockets in sea ice can shift the seasonal extrema in ice area and volume by up to several weeks. The GCMs also showed the mean distribution of the sea ice and its growth and melt rates were altered substantially. *Bitz and Lipscomb* (1999) updated the thermodynamic sea ice model of *Maykut and Untersteiner* (1971) to conserve energy and use faster numerics, and *Bitz et al.* (2001) noted that implementing this scheme is a small portion of the computational cost of running a full GCM. Nonetheless, it is still common for GCMs to use the Semtner (1976) zero-layer thermodynamics (e.g., MPI ECHAM5 and MRI-CGCM2.3.2, see Marsland et al., 2003 and Yukimoto et

al., 2006). Still other models use a multi-layer approach that restricts their influence to the upper ice layer after *Semtner* (1976) or *Winton* (2000) (e.g., GFDL 2.0 and 2.1 and CSIRO 3.0 and 3.5, see Delworth et al., 2006, and O'Farrell, 1998). Only two CMIP3 models (NCAR CCSM3 and PCM, see Holland et al., 2006) have adopted multi-layer thermodynamics with explicit brine-pocket physics.

Snow cover insulates the underlying sea ice from atmospheric temperature changes. Because snow has a higher albedo than sea ice, snow cover can delay the onset of summer melt. Land surface schemes include complex multi-layer representations of snow that allow freezing of surface melt and metamorphosis of the snow grain size. However, at this time we know of no GCM that has more than one resolved layer of snow properties on top of sea ice. One practical reason why snow physics in sea ice models has lagged behind its terrestrial counterpart is that each state variable in a sea ice model must be transported with the sea ice motion, and transport schemes with desirable numerical properties (e.g., high order, stable, and conservative) can be expensive. However, a new sea ice transport scheme that uses incremental remapping by *Lipscomb and Hunke* (2004) can efficiently transport large numbers of sea ice state variables.

The parameterization of melt ponds and radiative transfer in the sea ice and snow has been crude at best in GCMs until now. Heat and freshwater storage in melt ponds was ignored altogether in CMIP3 GCMs (as far as we know). Ponding was only considered to the extent that the surface albedo is typically a function of surface temperature: when melting, the surface albedo of bare sea ice is assigned a value that is meant to represent Arctic-wide conditions with some average pond fraction (e.g., *Briegleb et al.*, 2004). Yet a sophisticated physical treatment of melt ponds was implemented in a single-column sea ice model quite some time ago (*Ebert and Curry*, 1993). A GCM with explicit melt-pond mass and heat balance has been investigated with ECHAM5 (*Pedersen et al.*, 2009). The ponds substantially lowered the summer surface albedo and reduced the ice thickness.

A more consistent treatment of the radiative transfer through melt ponds and sea ice was developed in a one-dimensional sea ice model by *Taylor and Feltham* (2003). In this case a two-stream radiative transfer scheme was used to compute the surface albedo; absorption within the snow, ice, and pond; and transmission to the underlying ocean. Another radiative transfer method for sea ice and melt ponds (*Briegleb and Light*, 2007) incorporates a Delta-Eddington, multiple-scattering radiative transfer model to account for multiple scattering from snow grains, bubbles, and brine pockets. We anticipate that these new methods will soon appear in GCMs.

Another important aspect of sea ice physics is its varied distribution of thicknesses that exists on the scale of a typical GCM grid box. In a given region, sea ice thickness is best described by the probability density of ice thicknesses, known as the ice-thickness distribution (ITD). The ITD can be considered at the interface of thermodynamics and dynamics, as both class of

processes fundamentally alters the ITD time evolution. In models, the ITD is represented by a number of ice thickness categories (or bins), including open water, in each GCM grid cell. Growth and melt processes may shift the ice between categories or create new thin ice, while deformation tends to break up thin ice and raft it or pile it up into ridges, which broadens the probability distribution and creates a long tail of thick ice. An increase in the resolution of the ITD in a model increases the total ice volume (and thickness), and hence the freshwater transport by sea ice is greater (*Bitz et al.*, 2001; *Holland et al.*, 2001, 2006). Several GCMs implemented parameterizations of an ITD in their latest versions (e.g., NCAR CCSM3 and PCM, UKMO HADGEM1, GFDL 2.0 and 2.1, and CNRM-CM3, see Holland et al., 2006, McLaren et al., 2006, and Salas-Mélia, 2002).

2.2 Flux Adjustments, Ocean Parameterizations, and Grids

Flux adjustments were a common feature of models in the early ACSYS era, which have been subsequently eliminated in most GCMs. Flux adjustments are prescribed offsets added to the freshwater and/or heat flux. They are intended to account for deficiencies in the coupled simulation that cause drift in the ocean surface salinity and/or temperature. The offsets usually vary from month to month but repeat year to year, and they are estimated by computing the mismatch in surface fluxes that arise in uncoupled simulations of the atmosphere and ocean with prescribed surface boundary conditions (see e.g., *Manabe et al.*, 1991). Flux adjustment typically can be eliminated and a stable climate simulation can be achieved without them, by raising the ocean component's resolution and improving ocean mixing parameterizations (e.g., *Boville and Gent*, 1998; *Gordon et al.*, 2000). The elimination of flux adjustments is a positive step in improving climate models, as they have been shown to influence climate sensitivity (*Gregory and Mitchell*, 1997).

Many models also now incorporate a representation of the freshwater input to the Arctic Ocean from continental river inflow, which is important for the freshwater balance of the Arctic and the dynamics of the Arctic shelf areas. Schemes are often very simple, with runoff at the land surface as a result of snowmelt and rainfall less evapotranspiration in excess of the needs of the model's soil moisture intake. Runoff is routed into the ocean via defined basins defined by the model's surface topography.

Recent models without flux adjustments simulate the 20th century sea ice cover or Arctic surface air temperature with about the same fidelity as models with flux adjustments (e.g., *Flato*, 2004; *Hu et al.*, 2004). Among the models that do not have flux adjustments, many use a parameterization of advection by mesoscale eddies from *Gent and McWilliams* (1990) (GM). Poleward heat transport by ocean mesoscale eddies tends to be large in high southern latitudes, and some studies have found that using the GM parameterizations reduces the modeled sea ice extent in the Southern Hemisphere, but it has

little influence in the Northern Hemisphere (*Hirst et al.*, 2000; *Gent et al.*, 2002).

Many ocean models have progressed from the rigid-lid approximation (with zero vertical motion at the surface) to various free-surface formulations in the past decade or so (*Griffies et al.*, 2000). These new formulations permit more realistic exchange of mass, energy, and momentum across the ice-ocean interface. Even with the latest sea ice thermodynamic formulations that include brine-pockets, ice-thickness distribution and melt ponds, proper conservation is relatively straightforward (*Schmidt et al.*, 2004). Instabilities have been known to arise from the interaction of sea ice dynamics coupled to free surface formulations, but they can also be avoided with relatively simple solutions (*Schmidt et al.*, 2004).

Ocean and sea ice models often share the same grid and many global models in the past discretized their grid in spherical coordinates. The convergence of meridians at the North Pole demanded very small time steps, filtering small-scale variations in the zonal direction near the pole, and/or imposing an artificial island at the pole. *Griffies et al.* (2000) point out that filtering introduces noise and can destroy geostrophic and thermodynamic balances in ocean models. In sea ice models, filtering can create unphysical negative ice thicknesses and concentrations (*Moritz and Bitz*, 2000). Further the artificial "shadowing" of fluid flow around an artificial island is undesirable. During the ACSYS era much effort was placed on generalizing models to arbitrary orthogonal curvilinear coordinates, which permit coordinate singularities to be moved onto land. See *Griffies et al.* (2000) for a review of this practice in ocean models and *Hunke and Dukowicz* (1997) for an example in a sea ice model. Examples of CMIP3 models that use generalized orthogonal curvilinear coordinates are GFDL CM 2.0 and 2.1 and NCAR CCSM3 (*Delworth and et al.*, 2006; *Collins et al.*, 2006).

The Arctic Ocean Model Intercomparison Project (AOMIP; Proshutinsky et al., 2001) has provided a coordinated effort to validate and improve model simulations of the Arctic ocean. This has led to an improved understanding of the processes affecting Arctic ocean conditions and circulation and subsequent recommendations for model improvements. A recent special issue of the Journal of Geophysical Research - Oceans (Proshutinsky and Kowalik, 2007) highlights many of these studies. As one example, AOMIP studies have shown that tidal effects (which are not typically included in GCMs) can increase ventilation of the Atlantic layer and thereby increase its heat loss with subsequent impacts on the sea ice mass budget (Holloway and Proshutinsky, 2007). These studies suggest that Arctic ocean tidal effects have important climate consequences and should be incorporated in future GCM ocean model developments.

2.3 Atmospheric Circulation and Clouds

Many GCMs have a systematic bias in the atmospheric surface circulation in the Arctic with a tendency for the mean sea-level pressure to be too high over the Arctic Ocean, except in the Beaufort and Chukchi seas in winter, where it is too low (*Walsh and Crane*, 1992; *Walsh et al.*, 2002; *Chapman and Walsh*, 2007). The across model variance of sea level pressure in late 20th-century GCMs is larger in the Arctic than anywhere else in the Northern Hemisphere (*Walsh et al.*, 2002). *Bitz et al.* (2002) applied biases in the geostrophic winds derived from AMIP1 models to a sea ice model and showed that the sea-level pressure biases created severe errors in the sea ice thickness and ice transport in the Arctic. These sea ice errors in turn had a first-order influence on the freshwater exchange with the ocean surface.

Earlier intercomparison studies proved difficult at attributing biases in the sea level pressure to any particular model parameterization or resolution (*Bitz et al.*, 2002). With higher resolution models available now, *deWeaver and Bitz* (2006) found that surface winds gave rise to a better sea ice thickness pattern in one model at T85 resolution compared to T42 (about 1.4° compared to 2.8°).

Capturing the true vertical structure of the Arctic circulation in GCMs is also problematic. In at least one model, the Beaufort high in winter was found to have a baroclinic vertical structure, counter to the barotropic vertical structure in atmospheric reanalysis (*deWeaver and Bitz*, 2006). A study comparing synoptic patterns in CMIP3 models found that GCMs tend to have too frequent and too strong anticyclones in the Arctic winter (*Cassano et al.*, 2006).

The summertime Arctic surface circulation is dominated by a polar cyclone. The accompanying surface inflow and rising near the north pole, results in a deep (thermally indirect) Ferrel cell north of the well-known polar cell. These summertime features do not appear in most GCMs (*Bitz et al.*, 2002; *deWeaver and Bitz*, 2006). Such biases in the atmospheric circulation aloft are bound to influence the import of heat and moisture from lower latitudes and cloud formation in GCMs.

Clouds play an important role in climate regulation by absorbing and scattering solar and terrestrial radiation. In the Arctic, the role and effect of clouds on climate are more complex owing to the highly reflecting snow-ice surface, low temperatures, variable amounts of water vapor, and the surface-based wintertime temperature inversion (*Curry et al.*, 1996). Observations indicate that Arctic clouds act to warm the surface in winter and cool it for a short period in summer (*Shupe and Intrieri*, 2004).

Early GCM cloud schemes were often purely diagnostic and many adapted methods introduced by *Slingo* (1987) and *Wetherald and Manabe* (1988). Cloud fraction parameterizations typically depended on cloud type, which included convective and stratiform clouds (sometimes the latter was broken into a number of more specialized types). Cloud amounts usually depended on the

parameterized convective mass flux, temperature and relative humidity profiles, vertical velocity, and atmospheric stability. Cloud optical properties were either based on prescribed fields or they scaled with the vertically integrated water vapor (known as the precipitable water). Precipitation would result from condensation that forms under supersaturated (or nearly supersaturated) conditions. Condensate often fell immediately to the ground; although, it might be reduced somewhat by evaporation along its path. Whether the condensate was converted to snow usually depended on low-level temperature and often the latent heat of fusion was neglected.

In a thorough review of the state of knowledge of Arctic cloud processes, *Curry et al.* (1996) concluded that too little was known to properly model cloud feedback and that Arctic specific parametizations of clouds were needed in GCMs. Schemes for non-convective cloud schemes, which are the primary challenge in modeling Arctic clouds (*Curry et al.*, 1996), have seen improvements. A major step forward can be realized with the treatment of cloud liquid and ice condensate as prognostic variables — with individual equations that describe their evolution in time. Such schemes permit condensation prior to grid-box wide saturation and allow condensate to spend time within a cloud before converting to precipitation. These features are necessary to simulate ice condensate, which is needed to effectively dissipate moisture in winter. Because ice condensate grows larger and therefore falls faster than liquid condensate, proper mixed-phase cloud schemes are needed to accurately simulate cloud amount and optical properties (*Beesley and Moritz*, 1999). The MPI ECHAM4 model was among the first GCMs to adopt a prognostic cloud water scheme with explicit ice-phase physics (*Sundqvist et al.*, 1989), and the effort returned one of the best simulations of Arctic clouds among the 18 uncoupled atmosphere models analyzed by *Tao et al.* (1996).

Yet Arctic clouds in most GCMs have been a major source of error for decades. Uncoupled atmosphere models of the early ACSYS era had Arctic average cloud cover ranging from 30–90% in winter and 20–100% in summer, even though sea ice cover and SST boundary conditions were prescribed from observations (*Tao et al.*, 1996). In addition, *Tao et al.* (1996) found no association between variations in the across-model winter cloud cover and winter surface temperature. *Randall et al.* (1998) note that the absence of a positive correlation is counter to observations.

More mature and fully coupled models that participated in CMIP2 had a slightly narrower range in cloud cover, at 40–90% in winter and 40–80% in summer (among the 9 models that reported cloud cover, see Holland and Bitz, 2003). The most current CMIP3 models have not further narrowed the wintertime range, but the summertime cloud cover in 21 of the 23 models has narrowed to within 10% of the observed cover. Yet CMIP3 models are still puzzling, as there is now a weak but significant *negative* correlation between winter cloud cover and surface temperature across these newer models.

Some have argued that regional climate models (RCMs) offer a good platform for developing and testing parameterizations for GCMs, especially for

cloud and radiation processes because the large-scale evolution of atmospheric dynamics is constrained by prescribed lateral boundary conditions (*Wyser et al.*, 2007; *Dethloff et al.*, 2008). Yet at this time, cloud fraction in the Arctic has nearly as large a spread in RCMs as in GCMs. Interestingly, the correlation between observed and modeled surface radiation fluxes individually for longwave and shortwave radiation is much higher than for cloud fraction in RCMs. *Wyser et al.* (2007) argue that this is because Arctic clouds are frequently very thin, and thus radiation and cloud fraction are not well correlated. Further they found evidence that more work is needed to properly model the correct phase, size distribution, and ice crystal habit of cloud condensate. Models exist that include ice fog and diamond dust (e.g. *Girard and Blanchet*, 2001), but the parameterizations are yet to be included in GCMs. *Girard and Blanchet* (2001) suggest that diamond dust ought to induce a strong radiative warming at the surface, but based on SHEBA data, *Shupe and Intrieri* (2004) concluded that diamond dust has very little radiative impact.

2.4 Ice Sheet Modeling

A few GCMs have incorporated an ice sheet model (ISM) such that changes to the global climate in the GCM can interact with the shape and extent of a changing Greenland ice sheet. The interaction occurs through changes in surface albedo as the ice sheet retreats or advances over bare soil, elevation-temperature feedbacks, and through changes in the atmospheric and oceanic circulation (*Huybrechts et al.*, 2002; *Ridley et al.*, 2005; *Driesschaert et al.*, 2007; *Mikolajewicz et al.*, 2007). The coupled ISMs show that the Greenland ice sheet declines for almost all future forcing scenarios, and Greenland's ice melts complete within 1-3 thousand years in the fastest warming scenarios. If surface mass balance is considered alone, then it has been suggested (*Gregory and Huybrechts*, 2006) that a global temperature rise of 3°C could trigger an irreversible decline in the mass of the Greenland ice sheet. The resolution of the atmospheric component of GCMs is too coarse to resolve the steep ice sheet margins, a feature which is needed since the surface ablation is highest at the low elevations of the margins. Consequently, high resolution (10-20km) three-dimensional thermo-mechanical ISMs are coupled to the GCM. The coupling interface allows surface temperature and precipitation to provide the surface mass balance. The surface runoff combined with ice-berg calving, determined by the ice dynamics, passes fresh water to the ocean. Surface ablation combined with ice dynamics, provides a new ice sheet orography for the GCM which influences atmospheric dynamics and surface albedo. Results from coupled GCMs and ISMs show that even with the fastest warming scenarios, the ice sheet melt water has only a minor influence on the Atlantic thermohaline overturning circulation and that atmospheric dynamics change after $\sim$200 years of ice sheet decline. The inclusion of ISMs in GCMs allows for their influence on ocean salinity and sea level rise, and it provides a validation

of the carbon cycle and precipitation through comparison of ISM diagnostics with observed ice cores.

3 CMIP3 Model highlights

In this section we highlight the simulated Arctic climate in the late 20th century and mid 21st century in two state-of-the-art climate models that are part of the CMIP3 dataset, the NCAR CCSM3 and UKMO HadGEM1. These models made great strides in development during the ACSYS era. Here we explore the extent to which the development effort influences the model results.

We analyze the SRES A1B scenario for the 21st century where the rate of anthropogenic greenhouse gas emissions increases during the first half of the 21st century, and then slowly declines in the second half. We compare HadGEM1 and CCSM3 to the CMIP3 model mean (which includes the two models) and to observations, where possible. A list of CMIP3 models is given in table 1 and much more information about the model physics can be found at http://www-pcmdi.llnl.gov/ipcc/model_documentation/ipcc_model_documentation.php. Sea ice output from GISS model EH and NCAR PCM were not available in the CMIP3 model archive at the time we wrote this paper. The IPSL CM4 model is excluded from sea ice diagnostics because its sea ice thickness changed abruptly at year 2000 owing to a change in aerosol forcing (S. Denvil, Per. Comm.). The IAP FGOALS model is excluded from our analysis because the sea ice in that model is about twice as extensive as observed and the mean thickness in the Arctic is almost 10 m. A few other CMIP3 models are also known to have severe biases in the Arctic, especially in the sea ice. Nonetheless, we use all available models with equal weights in our multi-model ensemble mean except as noted below. Each model contributes about 5% to the mean and usually the extreme biases are not of a single sign, so the ensemble mean is not significantly affected by any one model.

The highlighted models, CCSM3 and HadGEM1, stand out as among the most advanced in their sea ice physics, which include the elastic-viscous-plastic rheology and an explicit ice-thickness distribution with deformation and redistribution *Bitz et al.* (2001); *Lipscomb* (2001). CCSM3 has sea ice with explicit brine pocket physics and a vertical temperature profile (*Bitz and Lipscomb*, 1999). At least one study has argued that CCSM3 and HadGEM1 have the most realistic pattern of present-day Arctic sea ice thickness among CMIP3 models (*Gerdes and Köberle*, 2007), and they are the only models that simulate recent Arctic summer ice retreat that is consistent with satellite observations (*Stroeve et al.*, 2007) (although other models might compare favorably if they had run larger ensembles). Both models have free-surface oceans and are free of flux adjustments. They have prognostic ice and liquid condensate cloud physics, and above average horizontal resolution in all components.

3.1 Late 20th Century Climate

We begin by describing the surface air temperature near the end of the 20th century. Figure 1a-c shows the annual mean bias in the models relative to the ECMWF 40-yr reanalysis (ERA-40) (*Uppala et al.*, 2005). The bias in CCSM3 in the Arctic is less than 2°C in most regions, except notably it is too warm by 3-4°C just north of Novaya Zemlya and too cold by a similar amount on Kamchutka and over southeastern Alaska. CCSM3 is also too cold by about 4-7°C in the Labrador Sea, around the southern coast of Greenland, and further southwards in the North Atlantic drift. HadGEM1 is about 4-8°C too cold in a large swath over northern Canada and Alask, stretching out over the western central Arctic and over eastern Asia. There are also cold spots over Novaya Zemlya and eastwards over northern Russia. HadGEM1 is also cold in the North Atlantic drift, but much less so than CCSM3.

The difference between the two models in the Barents Sea is likely due to the splitting of the West Spitzbergen current around Svalbard where the western branch sinks and flows to the north and the eastern branch encounters the Barents Sea shelf. HadGEM1 sends a greater portion of its warm Atlantic water west of Svalbard, whilst CCSM3 sends too much to the east, where it cannot sink at first and instead melts too much sea ice (*Jochum et al.*, 2008). This explanation is consistent with the pattern of net upward surface heat flux in the two models (see Figs. 2a-b). The net surface flux maps the convergence of ocean heat transport, assuming the change in heat stored in the ocean column is small. Unfortunately, observational climatologies of surface heat fluxes are not reliable enough in the Arctic and subpolar seas to compute biases in Fig. 2.

The cold bias in CCSM3 in the Labrador Sea coincides with much too extensive sea ice (see Fig. 3a) and 50-150W m^{-2} lower net surface heat flux than in HadGEM1 (see Figs. 2a-b). The net surface heat flux on the southern flank of the Gulf Stream is about 50W m^{-2} lower in CCSM3 than in HadGEM1, consistent with the more negative surface air temperature bias in this region in CCSM3. In the Pacific sector, the net surface heat flux in HadGEM1 is lower than in CCSM3 by about 25-50W m^{-2} and the sea ice is more extensive in HadGEM1.

The region with the largest surface air temperature bias in the CMIP3 model mean is in the Barents Sea and along the sea ice edge east of Greenland (see Fig. 1c). The sea ice edge is also on average too far south in this region in the CMIP3 models (see Fig. 3c). The across-model standard deviation in the annual mean surface air temperature varies most in the Nordic Seas and around Iceland (see Fig. 1d). It is also large in the marginal ice zones, especially in the Labrador Sea, Baffin Bay, and Davis Strait. The pattern was similar in CMIP1 models (see Fig 6b of *Walsh et al.*, 2002), but the CMIP1 models had considerably less variability in the Nordic seas. There is no apparent improvement in the model spread in surface air temperature from CMIP1 to CMIP3 when all models are considered from both eras. However,

generally the surface air temperature and ice extent biases are lower in this region in HadGEM1 and CCSM3. The net surface flux in Fig. 2 along the ice edge between Norway and the southern tip of Greenland in the CMIP3 model mean is much smaller than in HadGEM1 and CCSM3. Although we have not ruled out the role of the atmosphere in our analysis, we note that the greater convergence of heat by the ocean in the subpolar Atlantic in HadGEM1 and CCSM3 is likely a major factor in their higher quality simulations east of Greenland.

Figures 3a-c show the annual mean sea ice thickness. CCSM3 and HadGEM1 have much thicker ice than the CMIP3 model average (averages are given in Table 3). Despite colder surface air temperatures, HadGEM1 has thinner ice than CCSM3. Ice thickness is not observed uniformly in space, so we do not include a figure for comparison. However, HadGEM1 and CCSM3 agree more favorably with the sporadic measurements from submarine upward looking sonar (see, e.g., *Bourke and Garrett*, 1987; *Rothrock et al.*, 1999), with values derived from satellite altimetry data (*Laxon et al.*, 2003), and with a hindcast using an ice-ocean model forced with observed atmospheric conditions (*Gerdes and Köberle*, 2007). The build-up of thick ice along the Canadian Archipelago in the HadGEM1 and CCSM3 is most likely an indication of reasonable surface winds in the Arctic.

Figures 4a-c show the bias in the mean annual cycle of the zonal-mean surface air temperature in the models relative to the ERA40. The warm bias in CCSM3 in the Arctic is mostly a wintertime phenomena, reaching a maximum north of 70°N in late winter. The cold bias in CCSM3 is the worst at about 65°N in summer. There is a cold bias in HadGEM1 nearly year-round, but it is the worst in winter at all latitudes considered. The CMIP3 ensemble mean has a similar bias pattern though with slightly lower magnitude than HadGEM1.

In the across-model standard deviation computed for the zonal means by month (see Fig. 4d), the magnitude is largest in winter and at the highest latitudes. The maximum standard deviation is not at the transitions between melt/freeze periods. Instead the maximum variance is likely due to variations in downwelling longwave radiation associated with biases in the wintertime clouds and atmospheric heat transport, and associated biases in the ice thickness and/or snow depth.

The seasonal cycle in cloud cover is shown in Fig. 5. HadGEM1 is within a few percent of recently observed cloud cover in all months except May and Oct. CCSM3 matches the observations well from Jan-Apr, but its cloud cover is at least 10% too low the rest of the year. Both models simulate the mean annual cycle of cloud cover well compared to the average of the CMIP3 models. These modest cloud biases in HadGEM1 also do not help explain the large cold bias in that model.

We believe HadGEM1 and CCSM3 simulate some cloud properties relatively well compared to other CMIP3 models because they have mixed-phase cloud scheme that independently predict the ice and liquid water content in

clouds (*Collins et al.*, 2006; *Martin et al.*, 2006). Yet, cloud cover is only one cloud property of interest. *Gorodetskaya et al.* (2007) recently showed that despite relatively good agreement with summertime cloud fraction in CCSM3, the cloud liquid water content exceeds observed values, biasing cloud radiative properties. (*Gorodetskaya et al.* (2007) did not analyze HadGEM1.)

Model intercomparisons usually find that an across-model ensemble mean performs better than any individual model, especially for large-scale performance metrics (*Gleckler et al.*, 2008, e.g.,). However, the accuracy of many aspects of the Arctic climatology in HadGEM1 and CCSM3 is substantially better than the CMIP3 model mean. It is apparent that the efforts to improve these models has paid off.

3.2 Mid-21st Century Climate Change

The pattern of surface warming at mid-21st century in HadGEM1 and CCSM3 and in the CMIP3 model mean is shown in Figs. 6a-c. Clearly HadGEM1 and CCSM3 warm much more than the average CMIP3 model. All three panels have the largest warming over the sea ice on the Atlantic side of the Arctic Ocean. There is a complementary local maximum in the change in upward net surface heat flux in the same region (see Fig. 7). The magnitude is at least three times larger in HadGEM1 and CCSM3, consistent with the larger surface warming and sea ice retreat in these models (Fig. 7). The center of maximum warming in CCSM3 extends far deeper into the Arctic Ocean compared to HADGEM1. It is here where 20th-century perennial ice becomes seasonal by mid-21st century in CCSM3. *Arzel et al.* (2006) speculated that the large ice retreat in the Barents Sea in the 21st century on average in the CMIP3 models results from an increase in oceanic heat transport there. Our Fig. 7 confirms their suspicion.

There are other large differences in 21st-century net surface heat fluxes between CCSM3 and HadGEM1. The net surface heat flux increases by more than 30W m^{-2} in the Labrador Sea in the CCSM3 and the sea ice retreats at a high rate there, while the net surface heat flux change has the opposite sign in this region in HadGEM1 (and in the CMIP3 model mean). There is a 10-30W m^{-2} increase in heat flux along the North Pacific ice edge in HadGEM1, where in CCSM3 the heat flux increase is much less. We suspect these differences arise from major changes in the ocean circulation that are driven by shifts in the midlatitude jets, but we have not analyzed this in depth.

Table 2 lists the mid-21st century Arctic temperature change (75-90N), global mean temperature change, and their ratio, which we call the polar amplification. The highlighted models, HadGEM1 and CCSM3, are considerably higher in all three statistics than the CMIP3 model mean. These two models warm about 6°C on average from 75–90°N, which is more than three times the global mean.

The large warming in HadGEM1 and CCSM3 is also associated with relatively high thinning and retreat of sea ice in these models (see Figs. 8a-c). Area average sea ice statistics listed in Table 3 indicate that thickness and extent changes in HadGEM1 and CCSM3 are 50–100% larger than the CMIP3 model means. The more uniform surface warming over the Arctic Ocean in CCSM3 compared to HadGEM1 (Fig. 6), coincides with greater thinning across the Arctic Ocean in CCSM3. In contrast, in HadGEM1 the warming is sharply peaked at the ice edge in the Barents Sea, where there is also a large gradient in the change in upward net surface heat flux in that model.

It had been shown with CMIP2 models that sea ice thickness influences the Arctic response to increasing anthropogenic greenhouse forcing, while the extent has little or no influence (*Rind et al.*, 1995; *Holland and Bitz*, 2003; *Walsh and Timlin*, 2003). Across-model correlation analysis of these variables in the CMIP3 models is given in Table 4. With monthly mean output available in the CMIP3 archive, we are able to examine monthly relations. However, thickness anomalies are highly correlated from month to month (and year to year), so monthly thickness data are not needed. Table 4 indicates that across-models for the period 1980-199, the mean thickness is highly correlated with the mean extent in September but not April. Presumably this is because the summer surface energy balance has a large influence on ice thickness and summertime extent, while the winter extent is heavily influenced by wintertime winds and ocean heat fluxes (see *Bitz et al.*, 2005).

However, the positive across-model correlation between thickness and September extent does not carry-over to HadGEM1 and CCSM3. Instead these models have above average thickness but below average September extent (see Table 3). We believe that CCSM3 and HADGEM1 are unusual because they explicitly resolve the time evolution of the sea-ice thickness distribution (ITD) in their sea ice component models. When models resolve the ITD, the total ice volume in the Arctic increases (*Bitz et al.*, 2001; *Holland et al.*, 2001, 2006) and the ice thickness increases on average (over grid cells and larger regions). The ice extent seems to improve as well (*Bitz et al.*, 2001; *Salas-Mélia*, 2002). We suspect that most CMIP3 models have been compromised when tuning: If they had been tuned to be less extensive, they would also have become too thin. This compromise may be reduced when an ITD is included. In addition, the winter surface temperature tends to be slightly warmer when thin ice is resolved in regions with both perennial and firstyear ice. It is also apparent that HadGEM1 and CCSM3 have a larger annual range of sea ice area than the CMIP3 model mean, which is expected in models with an ITD (*Bitz et al.*, 2001; *Holland et al.*, 2001, 2006).

The across-model correlations in Table 4 that relate quantities in the late 20th century with the changes at mid 21st century are relevant for understanding relative changes in HadGEM1 and CCSM3 compared to the CMIP3 mean. Across CMIP3 models, we find that the September extent correlates significantly with the September retreat, such that models with more extensive ice retreat more slowly. Interestingly the opposite relation occurs in April,

albeit with a weaker correlation. Because the relations are seasonally opposing, the annual-mean extent is not well correlated with annual-mean retreat. One might imagine that models with thicker ice would retreat more slowly, but there is no significant correlation between these quantities because the models with thicker ice also have significantly more thinning. This unintuitive result stems from the fact that ice growth in winter damps anthropogenic thinning to some extent (*Bitz and Roe*, 2004). The growth rate is inversely related to ice thickness, and hence the thinner the ice, the more strongly damped is its rate of thinning. The argument holds provided the net damping dominates over the positive ice-albedo feedback, which must be so when and where sea ice is stable.

Figure 9 illustrates the probability density of the fractional sea ice coverage (which depicts the ITD) for the late 20th century and the mid and late 21st century. The two individual models have a tendency to lose multiyear ice and gain firstyear ice in the 21st century. In the late 20th century, CCSM3 has more multiyear (a larger thick-ice tail) than HadGEM1 (see Fig. 9). Yet the multiyear ice disappears sooner in CCSM3 than in HadGEM1, despite similar magnitudes of global and Arctic warming in the models. Also note that in CCSM3 compared to HadGEM1 by mid 21st century, the sea ice retreat in September retreat are is about 50% greater (see Table 3). Thus the multiyear sea ice cover appears to be more sensitive to warming in CCSM3 than HadGEM1.

Figure 10 shows the mean annual cycle of the change in zonal mean surface air temperature. The season of maximum warming is in early winter (Oct.–Nov.), when the CMIP3 model mean warms on average more than 6°C north of 80°N and HadGEM1 and CCSM3 warm more than 11°C. The warming is about 3-5°C lower in deep winter (Jan.–Mar.) in HadGEM1. In summer (Jun.–Aug.), the warming is a minimum (at 2°C or less) north of 70°N. Polar amplification is most apparent during the cold season, and it is absent during the melt season, because the temperature is limited to the melting temperature over a substantial portion of the Arctic.

Greater springtime warming in HadGEM1 may result from the larger increase in cloud cover in May (see Figs. 4 and 11). The larger cloud increase in Fall in CCSM3 could be a factor in the larger Fall surface air warming in CCSM3.

We end our analysis with a discussion of the atmospheric and ocean heat transport into the Arctic. The poles are sometimes referred to as heat sinks for the planet. Indeed about 100 W m^{-2} of heat escapes the top of the atmosphere on average north of 70°N over the year (*Oort*, 1974). About 2/3 of the atmospheric heat transport across 70°N is due to sensible heat and potential energy transport, known as the dry static energy (DSE) transport, and about 1/3 is due to latent energy (LE) transport, with kinetic energy making up a near-negligible contribution (*Overland and Turet*, 1994). The DSE transport is thought to depend strongly on the meridional temperature gradients, while the latent heat transport depends mostly on temperature (e.g.,

see *Oort*, 1974; *Held and Soden*, 2006). In a greenhouse warming climate, one expects the annual mean poleward temperature gradient to decrease on average owing to polar amplification of the warming, thus the DSE transport into the Arctic should decrease, giving rise to a negative feedback. At the same time, the rising temperature is expected to increase the LE transport into the Arctic. Figure 12 shows this expected behavior in HadGEM1, CCSM3, and the CMIP3 model mean. The sum of the two components in the CMIP3 model mean is near zero (see Fig. 12c). In contrast, the decrease in northward DSE transport is greater than the increase in northward LE transport in HadGEM1 and CCSM3, consistent with the very large polar amplifications in these two models.

Figure 12 also shows the change in northward oceanic heat transport. This quantity increases slightly north of 60°N in the CMIP3 model mean, and it increases a relatively much larger amount in HadGEM1 and CCSM3. An increase in the oceanic heat transport into the Arctic was found in the majority of CMIP2 models as well (*Holland and Bitz*, 2003). *Bitz et al.* (2006) analyzed this increase in CCSM3 and posited a positive feedback between ocean heat import into the Arctic and sea ice retreat. Thus the poleward ocean heat transport likely contributes to polar amplification in the Arctic surface warming at mid 21st century and may even be part of another positive feedback.

4 Summary and Future Outlook

A number of modeling centers have devoted a considerable amount of energy to improve high latitude climate physics in their models during the ACSYS era. In the best models the sea ice components now take into account the ice rheology, ice-thickness distribution, and multiple vertical layers. For the ocean component of coupled models generally, flux adjustments have been eliminated, terrestrial runoff schemes have been adopted, and vertical mixing schemes have been updated. There is some evidence that modeled atmospheric circulation benefits from higher resolution, and many models have implemented improved schemes for treating clouds.

Stimulated by the immense and immensely valuable CMIP3 archive, IPCC 2007 initiated a new paradigm in research with GCMs (*Meehl et al.*, 2007). With the model output archived substantially in advance, analysis included in the assessment could test hypothesis with a variety of GCMs at once. In addition, a more thorough model intercomparison was possible. In this Chapter, we have reviewed numerous valuable studies that analyzed the Arctic climate in the CMIP3 models. These studies have had a significant impact on understanding model behavior and will steer the development of new model physics.

In section 3 we featured results from two climate models that saw substantial improvements during the ACSYS era. The pay-off is clear. The large-scale

pattern of sea ice thickness in the Arctic is well represented, and the sea ice edge east of Greenland is positioned fairly well. Cloud cover is within about 10% of observations when averaged north of 70°N. In some ways HadGEM1 and CCSM3 capture the late 20th century Arctic climate better than the multi-model ensemble mean of the CMIP3 models. These two models appear to have reduced sea ice albedo tuning compromises by including better sea ice physics. Thus the multi-model ensemble mean may not be the best forecast in an area such as the Arctic, where model physics in some models lag severely behind the best models.

It is unfortunate that we were unable to examine each CMIP3 model with the same level of detail that we gave to HadGEM1 and CCSM3. We do not claim that these two models are the best models. Indeed different studies have found superior behavior in other CMIP3 models (e.g., *Chapman and Walsh*, 2007). They were chosen because we participated in their development.

These two models have considerably larger climate change in the Arctic than the multi-model ensemble mean by mid 21st century compared to the late 20th century. The surface warms by about 6°C on average north of 75°N in HadGEM1 and CCSM3, which is more than three times the global average. In contrast the surface warming in the CMIP3 model mean is less than 4°C, which is closer to twice the global average. The September sea ice extent declines by 4.2 and 6.2×10^6 km^2 in HadGem1 and CCSM3, respectively, compared to just 2.9×10^6 km^2 in the CMIP3 model mean. The reduction in annual mean thickness north of 70N is similarly higher at 1.06 and 1.45 m in HadGem1 and CCSM3, respectively, compared to just 0.67 m in the CMIP3 model mean. Generally the changes across-models can be attributed somewhat to the late-20th century mean state (see Table 4). Models with below average September extent and above average thickness (as in HadGEM1 and CCSM3), tend to also have larger sea ice changes. The 20th-century ice thickness and September extent in HadGEM1 and CCSM3 are a good match to observations, which gives us some confidence that their large future changes are plausible. Compared to the CMIP3 model mean, HadGEM1 and CCSM3 also have above average increases in ocean heat transport into the Arctic, which appears to contribute to the large climate change in the two models.

We expect it will not be long before almost every GCM has a dynamical sea ice component with an ice-thickness distribution that builds ridges under compression and shear. Non-continuum, or discrete element, sea ice models that split floes based on the theory of fracture mechanics are still on the distant horizon for GCMs. Solving a multi-layer thermodynamics scheme for the vertical temperature profile and subsequently for sea ice growth and melt is not computationally expensive compared to sea ice dynamics and transport schemes. Brine-pocket energy storage adds only a minor complication. New physically based methods for treating melt ponds and radiative transfer in sea ice are well developed. New efficient sea ice transport schemes are making more sophisticated treatment of sea ice and snow thermodynamics and the sea ice thickness distribution (and the associated expanding lists of state variables)

feasible in GCMs. Owing to the importance of these sea ice physics, which was discussed in Section 2, we expect many models will adopt them soon.

Expanding computing capacity within the next decade will permit much higher resolution GCMs. In the Arctic this is likely to be important for improving atmospheric circulation and the representation of ocean eddies. Simulated oceanic heat and freshwater transport could benefit a great deal. Many GCMs will soon have the capacity to run high resolution regional components embedded within them, which should be useful for further investigating the role of tides and eddies in Arctic climate.

Cloud models are beginning to resolve size distributions of ice and liquid cloud condensate as well as a variety of ice crystal habits. Their development is part of the continued long path towards higher-quality Arctic cloud simulations.

Another area that will see rapid development in the next decade is the treatment of ice sheets. So far ice sheets in GCMs have only dealt with the behavior of deep, cold land ice. The important roles of ice shelves and their grounding line, ice streams, and calving have not yet been considered. New ice sheet models are needed to incorporate their behavior. The potential critical influence of ice sheet decay on sea level rise and ocean circulation has called the attention of many modelers to this important new work.

GCMs are evolving into Earth System Models that couple physical and biogeochemical systems to model Earth's cycles of carbon and aerosols. Many of the problems of interest for Earth System Modeling involve the polar regions, so the continued development of new physics and new capability must not be carried out without special emphasis on their operation in the polar regions.

Acknowledgements

The authors gratefully acknowledge the support of the National Science Foundation through grants ATM0304662 and OPP0454843 (CMB) and OPP0084273 (MMH). We acknowledge the modeling groups, the Program for Climate Model Diagnosis and Intercomparison (PCMDI) and the WCRP's Working Group on Coupled Modelling (WGCM) for their roles in making available the WCRP CMIP3 multi-model dataset. Support for this dataset is provided by the Office of Science, U.S. Department of Energy.

References

Arzel, O., T. Fichefet, and H. Goosse, Sea ice evolution over the 20th and 21st centuries as simulated by the current AOGCMs, *Ocn. Mod.*, *12*, 401–415, 2006.

Beesley, J. A., and R. E. Moritz, Toward an explanation of the annul cycle of cloudiness over the arctic ocean, *J. Climate*, *12*, 395–415, 1999.

Bitz, C. M., and W. H. Lipscomb, An energy-conserving thermodynamic model of sea ice, *J. Geophys. Res.*, *104*, 15,669–15,677, 1999.

Bitz, C. M., and G. H. Roe, A mechanism for the high rate of sea-ice thinning in the arctic ocean, *J. Climate*, *18*, 3622–31, 2004.

Bitz, C. M., M. M. Holland, A. J. Weaver, and M. Eby, Simulating the ice-thickness distribution in a coupled climate model, *J. Geophys. Res.*, *106*, 2441–2464, 2001.

Bitz, C. M., J. C. Fyfe, and G. M. Flato, Sea ice response to wind forcing from amip models, *J. Climate*, *15*, 522–536, 2002.

Bitz, C. M., M. M. Holland, E. C. Hunke, and R. E. Moritz, On the maintenance of the sea-ice edge, *J. Climate*, *18*, 2903–2921, 2005.

Bitz, C. M., P. R. Gent, R. A. Woodgate, M. M. Holland, and R. Lindsay, The influence of sea ice on ocean heat uptake in response to increasing co2, *J. Climate*, *19*, 2437–2450, 2006.

Bourke, R. H., and R. P. Garrett, Sea ice thickness distribution in the arctic ocean, *Cold Regions Sci. and Tech.*, *13*, 259–280, 1987.

Boville, B. A., and P. R. Gent, The ncar climate system model, version one, *J. Climate*, *11*, 1115–1130, 1998.

Briegleb, B. P., and B. Light, *A Delta-Eddington multiple scattering parameterization for solar radiation in the sea ice component of the Community Climate System Model*, NCAR/TN-472+STR, 2007.

Briegleb, B. P., C. M. Bitz, E. C. Hunke, W. H. Lipscomb, and J. L. Schramm, *Scientific Description of the Sea Ice Component in the Community Climate System Model, version 3*, NCAR/TN-463+STR, 2004.

Budyko, M. I., The effect of solar radiatin variations on the climate of the earth, *Tellus*, *21*, 611–619, 1969.

Cassano, J. J., P. Uotila, and A. H. Lynch, Changes in synoptic weather patterns in the polar regions in the 20th and 21st centuries. Part 1. Arctic, *Int. J. Climatol.*, *26*, DOI: 10.1002/JOC.1306, 2006.

Chapman, W. L., and J. E. Walsh, Simulation of arctic temperature and pressure by global climate models, *J. Climate*, *20*, 609–632, 2007.

Collins, W. D., et al., The Community Climate System Model, Version 3, *J. Climate*, *19*, 2122–2143, 2006.

Comiso, J. C., SSM/I concentrations using the Bootstrap Algorithm, *Tech. Rep. RP 1380, 40pp*, NASA, Technical Report, 1995.

Curry, J. A., W. B. Rossow, D. Randall, and J. L. Schramm, Overview of arctic cloud and radiation charactereistics, *J. Climate*, *9*, 1731–64, 1996.

Delworth, T. L., and et al., Cm2 global coupled climate models - part 1: Formulation and simulation characteristics, *J. Climate*, *19*, 675–697, 2006.

Dethloff, K., A. Rinke, A. Lynch, W. Dorn, S. Saha, and D. Handorf, Chapter 8: Arctic regional climate models, in *Arctic Climate Change — The ACSYS Decade and Beyond*, p. this volume, 2008.

deWeaver, E., and C. M. Bitz, Atmospheric circulation and Arctic sea ice in CCSM3 at medium and high resolution, *J. Climate*, *19*, 2415–2436, 2006.

Driesschaert, E., T. Fichefet, H. Goosse, P. Huybrechts, L. Janssens, A. Mouchet, G. Munhove, V. Brovkin, and S. L. Weber, Modeling the influence of greenland ice sheet melting on the atlantic meridional overturning circulation during the next millennia, *Geophys. Res. Lett.*, *34 L10707*, doi:, 2007.

Ebert, E. E., and J. A. Curry, An intermediate one-dimensional thermodynamic sea ice model for investigating ice-atmosphere interactions, *J. Geophys. Res.*, *98*, 10,085–10,109, 1993.

Fichefet, T., and M. Morales Maqueda, Sensitivity of a global sea ice model to the treatment of ice thermodynamics and dynamics, *J. Geophys. Res.*, *102*, 12,609–12,646, 1997.

Flato, G. M., Sea-ice climate and sensitivity as simulated by several global climate models, *Clim. Dyn.*, *23*, 229–241, 2004.

Flato, G. M., and W. D. Hibler, Modeling pack ice as a cavitating fluid, *J. Phys. Oceanogr.*, *22*, 626–651, 1992.

Gent, P. R., and J. C. McWilliams, Isopycnal mixing in ocean circulation models, *J. Phys. Oceanogr.*, *20*, 150–155, 1990.

Gent, P. R., A. P. Craig, C. M. Bitz, and J. W. Weatherly, Parameterization improvements in an eddy-permitting ocean model, *J. Climate*, *13*, 1447–1459, 2002.

Gerdes, R., and C. Köberle, Comparison of arctic sea ice thickness variability in IPCC climate of the 20th century experiments and in ocean sea ice hindcasts, *J. Geophys. Res.*, *112*, C04S13, doi:10.1029/2006JC003,616, 2007.

Girard, E., and J. P. Blanchet, Simulation of arctic diamond dust, ice fog, and thin stratus using an explicit aerosol-cloud-radiation model, *J. Atmos. Sci.*, *58*, 1199–1221, 2001.

Gleckler, P. J., K. E. Taylor, and C. Doutriaux, Performance metrics for climate models, *J. Geophys. Res.*, *113*, D06,104, doi:10.1029/2007JD008,972, 2008.

Gordon, C., C. Cooper, C. A. Senior, H. T. Banks, J. M. Gregory, T. C. Johns, J. F. B. Mitchell, and R. A. Wood, The simulation of SST, sea ice extents and ocean heat transports in a version of the Hadley Centre coupled model without flux adjustments, *Clim. Dyn.*, *16*, 147–168, 2000.

Gordon, H. B., and S. P. O'Farrell, Transient climate change in the CSIRO coupled model with dynamics sea ice, *Mon. Wea. Rev.*, *125*, 875–907, 1997.

Gorodetskaya, I. V., L.-B. Tremblay, B. Lipert, M. A. Cane, and R. I. Cullather, Modification of the arctic ocean short-wave radiation budget due to

cloud and sea ice properties in coupled models and observations, *J. Climate*, *20*, 2007.

Gregory, J. M., and P. Huybrechts, Ice-sheet contributions to future sea-level change, *Phil. Trans. Royal Soc. A*, *364*, 1709–1731, 2006.

Gregory, J. M., and J. F. B. Mitchell, The climate response to co2 of the hadley centre coupled aogcm with and without flux adjustment, *Geophys. Res. Lett.*, *24*, 1943–1946, 1997.

Griffies, S. M., C. Böning, F. O. Bryan, E. P. Chassingnet, R. Gerdes, H. Hasumi, A. Hirst, A.-M. Treguier, and D. Webb, Developments in ocean climate modeling, *Ocean Modelling*, *2*, 123–190, 2000.

Hahn, C. J., and S. G. Warren, A gridded climatology of clouds over land (1971-96) and ocean (1954-97) from surface observations worldwide, *Tech. Rep. Documentation, 70pp*, Carbon Dioxide Information Analysis Center (CDIAC), Department of Energy, Oak Ridge, Tennessee, 2007.

Held, I. M., and B. J. Soden, Robust responses of the hydrological cycle to global warming, *J. Climate*, *19*, 5686–5699, 2006.

Hewitt, C. D., C. S. Senior, and J. Mitchell, The impact of dynamic sea-ice on the climate sensitivity of a GCM: A study of past, present, and future climates, *Clim. Dyn.*, *17*, 655–668, 2001.

Hibler, W. D., A dynamic thermodynamic sea ice model, *J. Phys. Oceanogr.*, *9*, 815–846, 1979.

Hibler, W. D., Modeling a variable thickness ice cover, *Mon. Wea. Rev.*, *108*, 1943–1973, 1980.

Hibler, W. D., The role of sea ice dynamics in modeling CO_2 increases, in *Climate Processes and Climate Sensitivity*, edited by J. E. Hansen and T. Takahashi, pp. 238–253, Geophysical Monograph 29, V 5, American Geophysical Union, 1984.

Hirst, A. C., S. P. O'Farrell, and H. B. Gordon, Comparison of a coupled oceanatmosphere model with and without oceanic eddy-induced advection. Part I: Ocean spinup and control integrations, *J. Climate*, *13*, 139–163, 2000.

Holland, D. M., L. A. Mysak, D. K. Manak, and J. M. Oberhuber, Sensitivity study of a dynamic thermodynamic sea ice model, *J. Geophys. Res.*, *98*, 2561–2586, 1993.

Holland, M. M., and C. M. Bitz, Polar amplification of climate change in the Coupled Model Intercomparison Project, *Clim. Dyn.*, *21*, 221–232, 2003.

Holland, M. M., C. Bitz, and A. Weaver, The influence of sea ice physics on simulations of climate change, *J. Geophys. Res.*, *106*, 2441–2464, 2001.

Holland, M. M., C. M. Bitz, E. C. Hunke, W. H. Lipscomb, and J. L. Schramm, Influence of the sea ice thickness distribution on polar climate in CCSM3, *J. Climate*, *19*, 2398–2414, 2006.

Holloway, G., and A. Proshutinsky, Role of tides in Arctic ocean/ice climate, *J. Geophys. Res.*, *112*, C04S06, doi:10.1029/2006JC003,643, 2007.

Hu, Z.-Z., S. I. Kuzmina, L. Bengtsson, and D. M. Holland, Sea-ice change and its connection with climate change in the arctic in CMIP2 simulations, *J. Geophys. Res.*, *109*, D10,106, doi:10.1029/2003JD004,454, 2004.

Hunke, E. C., and J. K. Dukowicz, An elastic-viscous-plastic model for sea ice dynamics, *J. Phys. Oceanogr.*, *27*, 1849–1867, 1997.

Hunke, E. C., and Y. Zhang, Comparison of sea ice dynamics models at high resolution, *Mon. Wea. Rev.*, *127*, 396–408, 2000.

Huwald, H., L.-B. Tremblay, and H. Blatter, A multilayer sigma-coordinate thermodynamic sea ice model: Validation against Surface Heat Budget of the Arctic Ocean (SHEBA)/Sea Ice Model Intercomparison Project Part 2 (SIMIP2) data, *J. Geophys. Res.*, *110*, C05,010, doi:10.1029/2004JC002,328, 2005.

Huybrechts, P., I. Janssens, C. Pocin, and T. Fichefet, The response of the greenland ice sheet to climate changes in the 21st century by interactive coupling of an aogcm with a thermomechanical ice-sheet model, *Annals Glac.*, *34*, 408–415, 2002.

IPCC, *Climate Change 1992: The IPCC Scientific Assembly Supplementary Report*, Cambridge University Press, Cambridge, UK, 198pp, 1992.

IPCC, *Climate Change 2007 The Physical Science Basis. Contribution of Working Group I to the Fourth Assessment Report of the Intergovernmental Panel on Climate Change*, Cambridge University Press, Cambridge, UK, 996pp, 2007.

Jochum, M., G. Danabasoglu, M. M. Holland, Y. Kwon, and W. Large, Ocean viscosity and climate, *J. Geophys. Res.*, *113, C06017*, doi:10.1029/2007JC004,515, 2008.

Kreyscher, M., M. Harder, P. Lemke, and G. M. Flato, Results of the Sea Ice Model Intercomparison Project: Evaluation of sea ice rheology schemes for use in climate simulations, *J. Geophys. Res.*, *105*, 11,299–11,320, 2000.

Laxon, S., N. Peacock, and D. Smith, High interannual variability of sea ice thickness in the Arctic region, *Nature*, *425*, 947–950, 2003.

Lemke, P., W. Owens, and W. Hibler, A coupled sea ice-mixed layer-pycnocline model for the weddell sea, *J. Geophys. Res.*, *95*, 9513–9525, 1990.

Lemke, P., W. Hibler, G. Flato, M. Harder, and M. Kreyscher, On the improvement of sea ice models for climate simulations: the sea ice model intercomparison project, *Ann. Glaciol.*, *25*, 183–187, 1997.

Lipscomb, W. H., Remapping the thickness distribution in sea ice models, *J. Geophys. Res.*, *106*, 13,989–14,000, 2001.

Lipscomb, W. H., and E. C. Hunke, Modeling sea ice transport using incremental remapping, *Mon. Wea. Rev.*, *132*, 1341–1354, 2004.

Manabe, S., R. J. Stouffer, M. J. Spellman, and K. Bryan, Transcient responses of a coupled ocean-atmosphere model to gradual changes of atmospheric CO_2. Part I. Annual mean response, *J. Climate*, *4*, 785–818, 1991.

Marsland, S. J., H. Haak, J. H. Jungclaus, M. Latif, and F. Roeske, The max-planck-institute global ocean/sea ice model with orthogonal curvilinear coordinates, *Ocean Modelling*, *5*, 91–127, 2003.

Martin, G., M. Ringer, V. Pope, A. Jones, C. Dearden, and T. Hinton, The physical properties of the atmosphere in the new Hadley Centre Global Environmental Model, HadGEM1. Part 1: Model description and global climatology, *J. Climate*, *19*, 147–168, 2006.

Maykut, G. A., and N. Untersteiner, Some results from a time-dependent thermodynamic model of sea ice, *J. Geophys. Res.*, *76*, 1550–1575, 1971.

McFarlane, N. A., G. J. Boer, J.-P. Blanchet, and M. Lazare, The Canadian Climate Centre second-generation general circulation model and its equilibrium climate, *J. Climate*, *5*, 1013–1044, 1992.

McLaren, A. J., et al., Evaluation of the sea ice simulation in a new coupled atmosphere-ocean climate model (HadGEM1), *J. Geophys. Res.*, *111*, C12,014, doi:10.1029/2005JC003,033, 2006.

Meehl, G. A., G. Boer, C. Covey, M. Latif, and R. Stouffer, Coupled Model Intercomparison Project, *Bull. Amer. Meteor. Soc.*, *81*, 313–318, 2000.

Meehl, G. A., C. Covey, T. Delworth, M. Latif, B. McAvaney, J. F. B. Mitchell, R. J. Stouffer, and K. E. Taylor, The WCRP CMIP3 multimodel dataset: A new era in climate change research, *Bull. Amer. Meteor. Soc.*, pp. DOI:10.1175/BAMS–88–9–1383, 2007.

Mikolajewicz, U., M. Vizcaino, J. Jungclaus, and G. Schurgers, Effect of ice sheet interactions in anthropogenic climate change simulations, *Geophys. Res. Lett.*, *34 L18706*, doi:, 2007.

Moritz, R. E., and C. M. Bitz, Climate model underestimates natural variability of Northern Hemisphere sea ice extent, *Science*, *288*, 927a, 2000.

Oberhuber, J. M., Simulation of the Atlantic circulation with a coupled sea-ice-mixed layer-isopycnical general circulation model. Part I: model description, *J. Phys. Oceanogr.*, *23*, 808–829, 1993.

O'Farrell, S. P., Investigation of the dynamic sea-ice component of a coupled atmosphere sea-ice general circulation model, *J. Geophys. Res.*, *103*, 15,751–15,782, 1998.

Oort, A. H., Year-to-year variations in the energy balance of the arctic atmosphere, *J. Geophys. Res.*, *79*, 1253–1260, 1974.

Overland, J. E., and P. Turet, Variability of the atmospheric energy flux across 70 N computed from the GFDL data set, in *Polar Oceans and their role in shaping the global environment*, edited by O. M. Johannessen, R. D. Muench, and J. E. Overland, Goephys. Monograph 85, American Geophysical Union, 1994.

Pedersen, C. A., E. Roeckner, M. Lüthje, and J.-G. Winther, A new sea ice albedo scheme including melt ponds for ECHAM5 general circulation model, *J. Geophys. Res.*, *114*, doi:10.1029/2008JD010,440, 2009.

Pollard, D., and S. L. Thompson, Sea-ice dynamics and co_2 sensitivity in a global climate model, *Atm. Ocean*, *32*, 449–467, 1994.

Proshutinsky, A., and Z. Kowalik, Preface to special section on Arctic Ocean Model Intercomparison Project (AOMIP) studies and results, *J. Geophys. Res.*, *112*, C04S01 10.1029/2006JC004,017, 2001.

Proshutinsky, A., et al., The Arctic Ocean Model Intercomparison Project (AOMIP), *EOS, Trans., Amer. Geophys. Union*, *82 (51)*, 637–644, 2001.

Randall, D., et al., Status of and outlook for large-scale modeling of atmosphere-ice-ocean interactions in the arctic, *Bull. Amer. Meteor. Soc.*, *79*, 197–219, 1998.

Ridley, J. K., P. Huybrechts, J. M. Gregory, and J. A. Lowe, Elimination of the greenland ice sheet in a high co2 climate, *J. Climate*, *18*, 3409–3427, 2005.

Rind, D., R. Healy, C. Parkinson, and D. Martinson, The role of sea ice in $2XCO_2$ climate model sensitivity. 1. The total influence of sea ice thickness and extent, *J. Climate*, *8*, 449–463, 1995.

Rothrock, D. A., Y. Yu, and G. A. Maykut, Thinning of the arctic sea ice cover, *Geophys. Res. Lett.*, *26*, 3469–3472, 1999.

Salas-Mélia, D., A global coupled sea ice-ocean model, *Ocean Modelling*, *4*, 137–172, 2002.

Schmidt, G. A., C. M. Bitz, U. Mikolajewicz, and L. B. Tremblay, Ice-ocean boundary conditions for coupled models, *Ocean Modelling*, *7*, 59–74, doi:10.1016/S1463–5003(03)00,030–1, 2004.

Sellers, W. D., A global climate model based on the energy balance of the earth-atmosphere system, *J. Appl. Meteor.*, *8*, 392–400, 1969.

Semtner, A. J., A model for the thermodynamic growth of sea ice in numerical investigaions of climate, *J. Phys. Oceanogr.*, *6*, 379–389, 1976.

Shupe, M. D., and J. M. Intrieri, Cloud radiative forcing of the arctic surface: The influence of cloud properties, surface albedo, and solar zenith angle, *J. Climate*, *17*, 616–628, 2004.

Slingo, J. M., The development and verification of a cloud prediction scheme for the ECMWF model, *Quart. J. Royal Met. Soc.*, *113*, 899–927, 1987.

Stroeve, J., M. M. Holland, W. Meier, T. Scambos, and M. Serreze, Arctic sea ice decline: Faster than forecast, *Geophys. Res. Lett.*, *34*, doi:10.1029/2007GL029,703, 2007.

Sundqvist, H., E. Berge, and J. E. Kristjánsson, Condensation and cloud parameterization studies with a mesoscale numerical weather prediction model, *Mon. Wea. Rev.*, *117*, 1641–1657, 1989.

Tao, X., J. E. Walsh, and W. L. Chapman, An assessment of global climate model simulations of arctic air temperatures, *J. Climate*, *9*, 1060–1075, 1996.

Taylor, P. D., and D. L. Feltham, A model of melt pond evolution on sea ice, *J. Geophys. Res.*, *109*, C12,007, doi:10.1029/2004JC002,361, 2003.

Uppala, S., et al., The ERA-40 re-analysis, *Quart. J. Roy. Meteor. Soc.*, *131*, 2961–3012, 2005.

Vavrus, S. J., The response of the coupled Arctic sea ice-atmosphere system to orbital forcing and ice motion at 6 ka and 115 ka BP, *J. Climate*, *12*, 873–896, 1999.

Vavrus, S. J., and S. Harrison, The impact of sea-ice dynamics on the Arctic climate system, *Clim. Dyn.*, *20*, 741–757, 2003.

Walsh, J., and M. Timlin, Northern Hemisphere sea ice simulations by global climate models, *Polar Res.*, *22*, 75–82, 2003.

Walsh, J. E., and R. G. Crane, A comparison of gcm simulations of Arctic climate, *Geophys. Res. Lett.*, *19*, 29–32, 1992.

Walsh, J. E., V. M. Kattsov, W. L. Chapman, V. Govorkova, and T. Pavlova, Comparison of arctic climate simultations by uncoupled and coupled global models, *J. Climate*, *15*, 1429–1446, 2002.

Wang, M., J. E. Overland, V. Kattsov, J. E. Walsh, X. Zhang, and T. Pavlova, Intrinsic versus forced variation in coupled climate model simulations over the arctic during the twentieth century, *J. Climate*, *20*, DOI:10.1175/JCLI4043.1, 1093–1107, 2007.

Washington, W. M., and G. A. Meehl, Climate sensitivity due to increased co_2: Experiments with a coupled atmosphere and ocean general circulation model, *Clim. Dyn.*, *8*, 211–223, 1989.

Wetherald, R., and S. Manabe, Cloud feedback processes in a general circulation model, *J. Atmos. Sci.*, *45*, 1397–1415, 1988.

Winton, M., A reformulated three-layer sea ice model, *J. Atmos. Ocean. Technol.*, *17*, 525–531, 2000.

Wolff, J.-O., E. Maier-Reimer, and S. legutke, The Hamburg ocean primitive equation model, *Tech. Rep. No. 13*, Tech. Rep., No. 13, German Climate Computer Center (DKRZ), Hamburg, 98 pp, 1997.

Wyser, K., et al., An evaluation of arctic cloud and radiation processes during the SHEBA year: Simulation results from eight arctic regional climate models, *Clim. Dyn.*, *22*, DOI 10.1007/s00,382–007–0286–1, 2007.

Yukimoto, S., A. Noda, T. Uchiyama, and S. Kusunoki, Climate Change of the twentieth through twenty-first centuries simulated by the MRI-CGCM2.3, *Papers in Meteorology and Geophysics*, *56*, 9–24, 2006.

Zhang, J., and D. Rothrock, Modeling arctic sea ice with an efficient plastic solution, *J. Geophys. Res.*, *108*, 3325–3338, 2000.

Zhang, X., and J. E. Walsh, Toward a seasonally ice-covered Arctic Ocean: Scenarios from the IPCC AR4 model simulations, *J. Climate*, *19*, 1730–1747, 2006.

Table 1. CMIP3 Models used in this study

Modeling Center	Model Abbreviations
Bjerknes Centre for Climate Research (Norway)	BCCR BCM2.0
Canadian Centre for Climate Modelling and Analysis (Canada)	CCCMA CGCM3.1 T47, T63
Centre National de Recherches Meteorologiques, Meteo-France (France)	CNRM CM3
Commonwealth Scientific and Industrial Research Organization (Australia)	CSIRO MK3.0, MK3.5
Geophysical Fluid Dynamics Laboratory (USA)	GFDL CM2.0, CM2.1
Goddard Institute for Space Studies (USA)	GISS AOM, EH, ER
Institute for Numerical Mathematics (Russia)	INMCM3.0
Institut Pierre Simon Laplace (France)	IPSL CM4
Center for Climate System Research (Japan)	MIROC3.2 MEDRES, HIRES
University of Bonn (Germany)	MIUB ECHO G
Max-Planck-Institut fuer Meteorologie (Germany)	MPI ECHAM5
Meteorological Research Institute (Japan)	MRI CGCM3.2.2A
National Center for Atmospheric Research (USA)	NCAR PCM, CCSM3
United Kingdom Meteorological Office (UK)	UKMO HADCM3, HADGEM1

Table 2. Change in mean temperature north of 75°N (ΔT_a), change in mean global temperature (ΔT_g), and Polar Amplification (PA=$\Delta T_a/\Delta T_g$). The change is the mean of 2040-2059 minus 1980-1999.

Model	ΔT_a	ΔT_g	PA
	deg C	deg C	
CCSM3	6.07	1.84	3.30
HADGEM1	5.72	1.71	3.35
CMIP3 Mean	3.67	1.59	2.35

Table 3. Northern Hemisphere Sea Ice Extent (SIE) and annual mean Sea Ice Thickness averaged north of 70N (SIT). The first series (without the Δ symbol) are means from 1980-1999. The second series (with the Δ symbol) is the mean of 2040-2059 minus mean of 1980-1999.

Model	Sep. SIE	Apr. SIE	SIT	Sep. ΔSIE	Apr. ΔSIE	ΔSIT
	10^6 km^2	10^6 km^2	m	10^6 km^2	10^6 km^2	m
CCSM3	7.5	16.8	2.13	-6.2	-2.9	-1.45
HADGEM1	7.3	17.3	2.11	-4.2	-2.8	-1.06
CMIP3 Mean	7.7	16.4	1.72	-2.9	-1.6	-0.67
Observations	7.1	15.0				

Table 4. Across-model correlations of sea ice variables as defined in Table 3. MIROC HIRES is eliminated from correlations that involve the change at mid 21st century, because the ice melts away in that model by about 2020, 60 years earlier than in any other model. Numbers in bold are significant at the 5% confidence level.

	Sep. SIE	Apr. SIE	SIT	Sep. ΔSIE	Apr. ΔSIE	ΔSIT
Sep. SIE				**0.52**	**0.40**	-0.19
Apr. SIE	0.18			-0.02	**-0.42**	0.18
SIT	**0.80**	0.02		0.30	0.17	**-0.58**

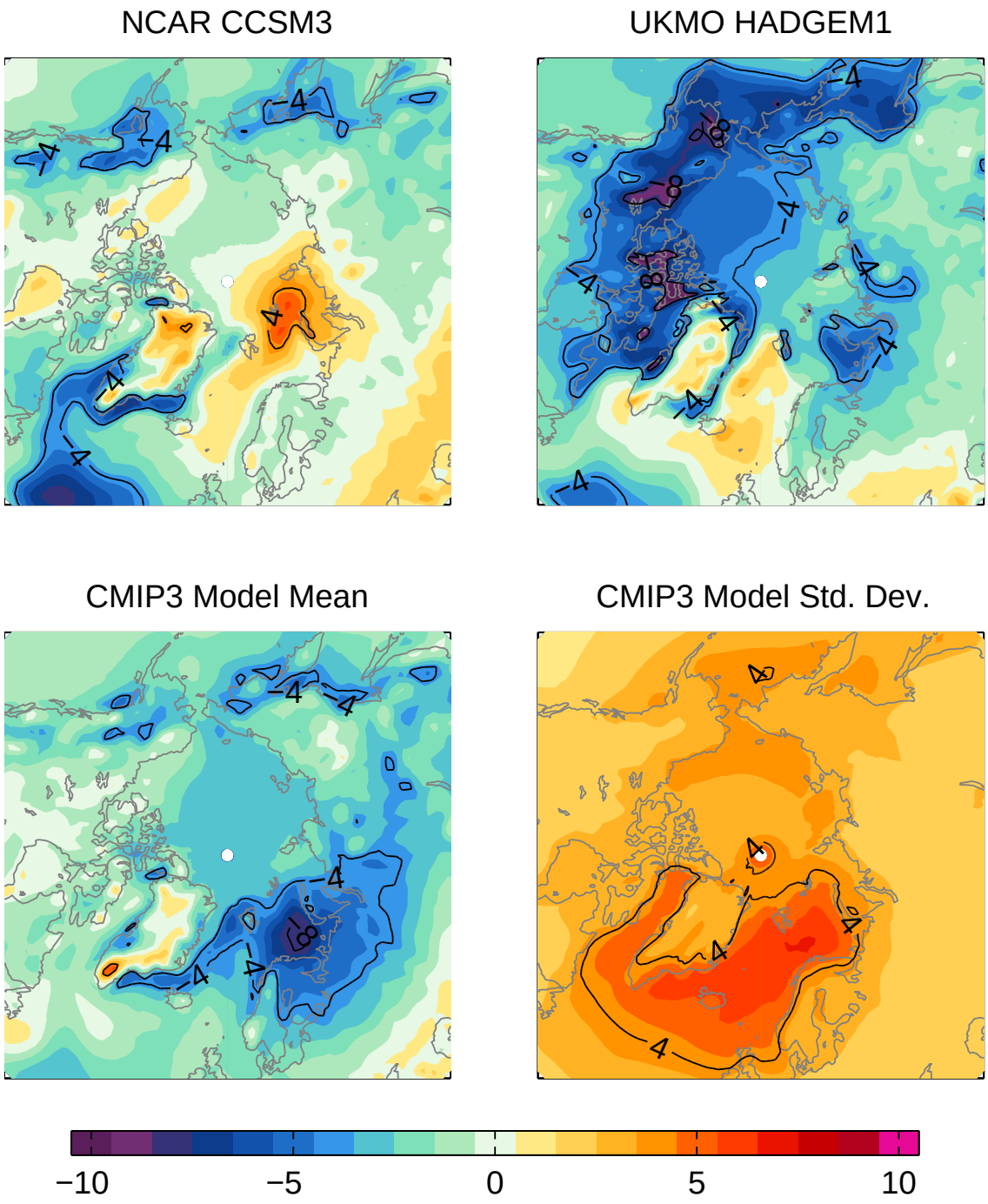

Fig. 1. 1980-1999 mean bias (a-c) and across-model standard deviation (d) of the 2 m surface air temperature. The bias is relative to observations from ERA-40.

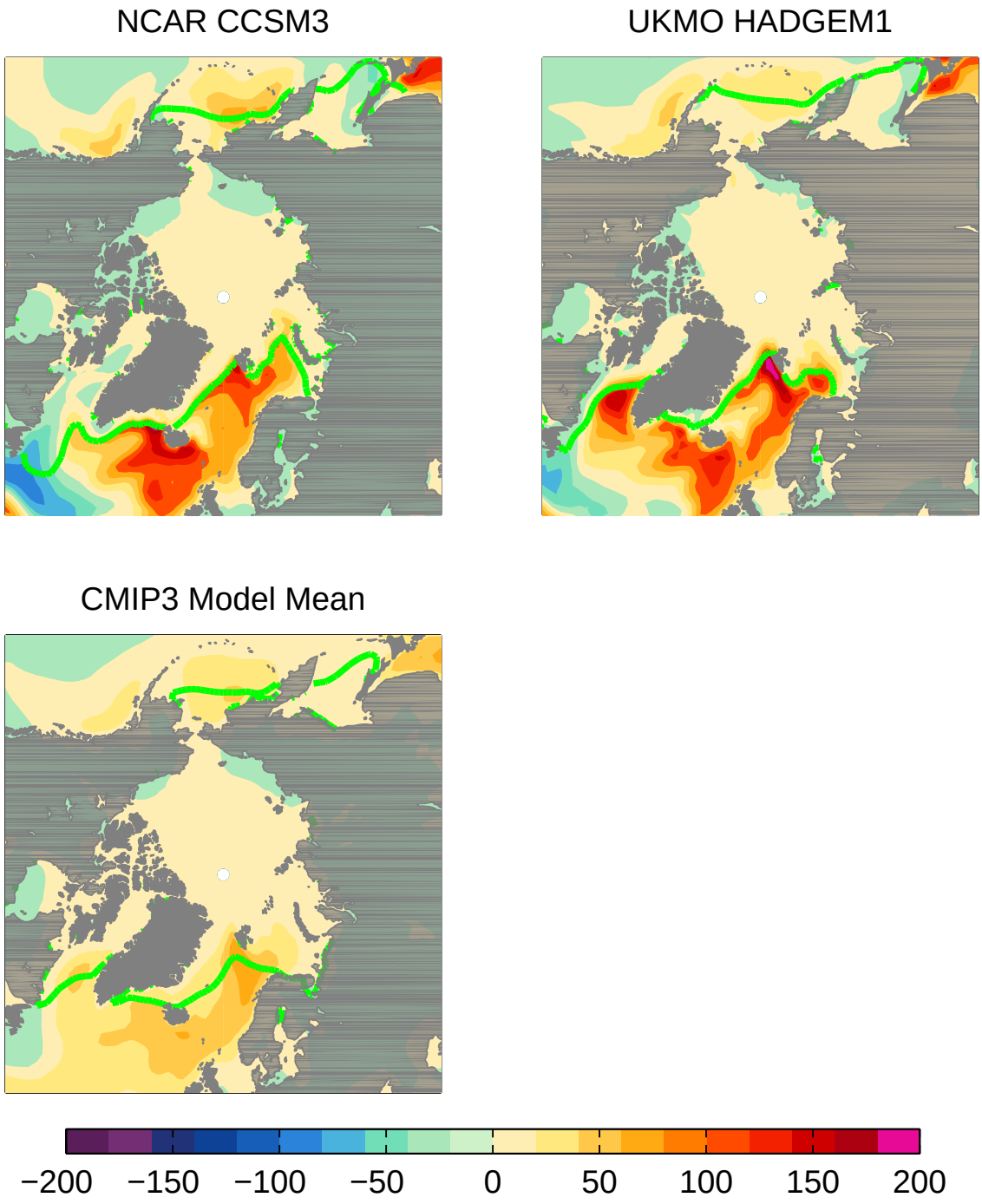

Fig. 2. 1980-1999 mean net upward surface heat flux and sea ice extent in the models (a-c). Ice extent is defined as the 15% concentration contour.

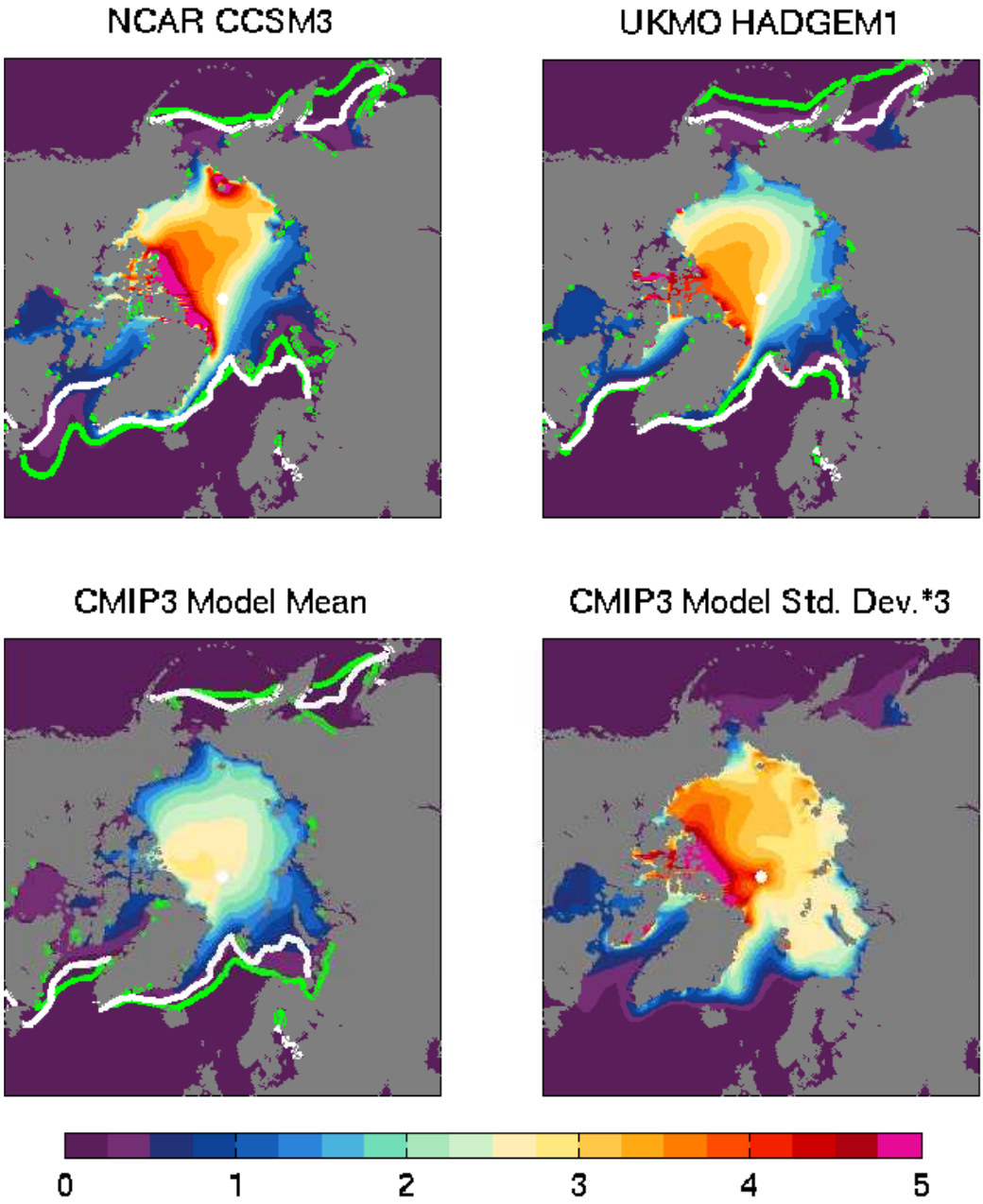

Fig. 3. 1980-1999 mean sea ice thickness (in m) and annual mean ice extent from the models (green line) with observed ice extent (white line) (a-c) and standard deviation of annual mean sea ice thickness scaled by a factor of 3 (d). Observations are from *Comiso* (1995). Ice extent is defined as the 15% concentration contour.

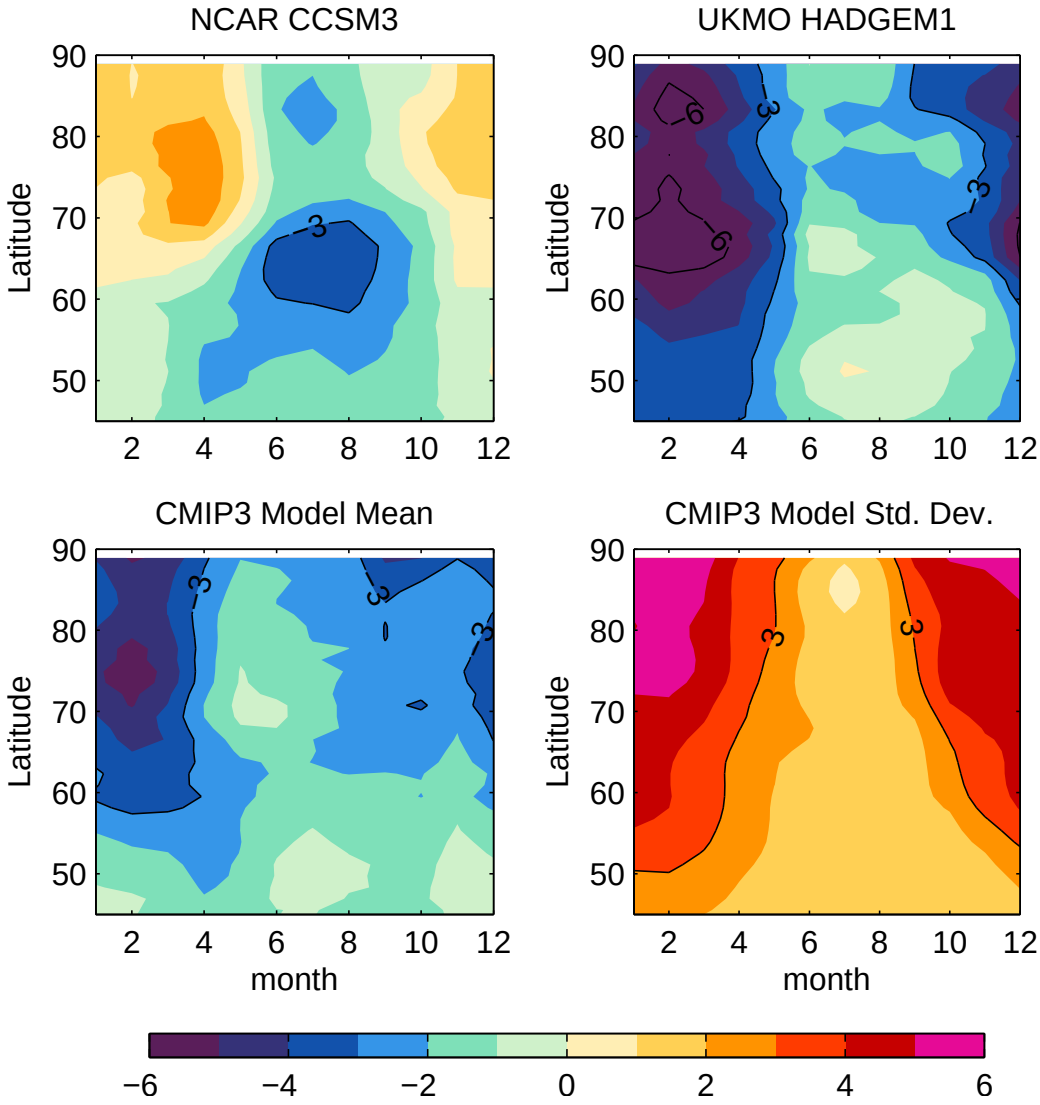

Fig. 4. 1980-1999 bias of the mean annual cycle of the zonally averaged 2 m surface air temperature (a-c) and across-model standard deviation (d) in °C. The bias is relative to observations from ERA40.

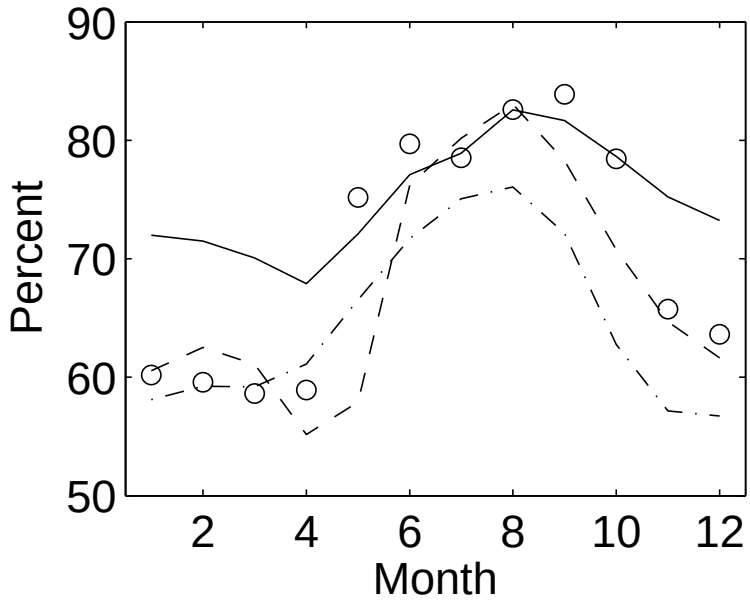

Fig. 5. 1980-1999 total cloud cover averaged 70-90°N. Lines indicate model results: dot-dashed for CCSM3, dashed for HADGEM1, and solid for CMIP3 Model Mean. Circles indicate observations, which are for the period 1954-1997 from *Hahn and Warren* (2007).

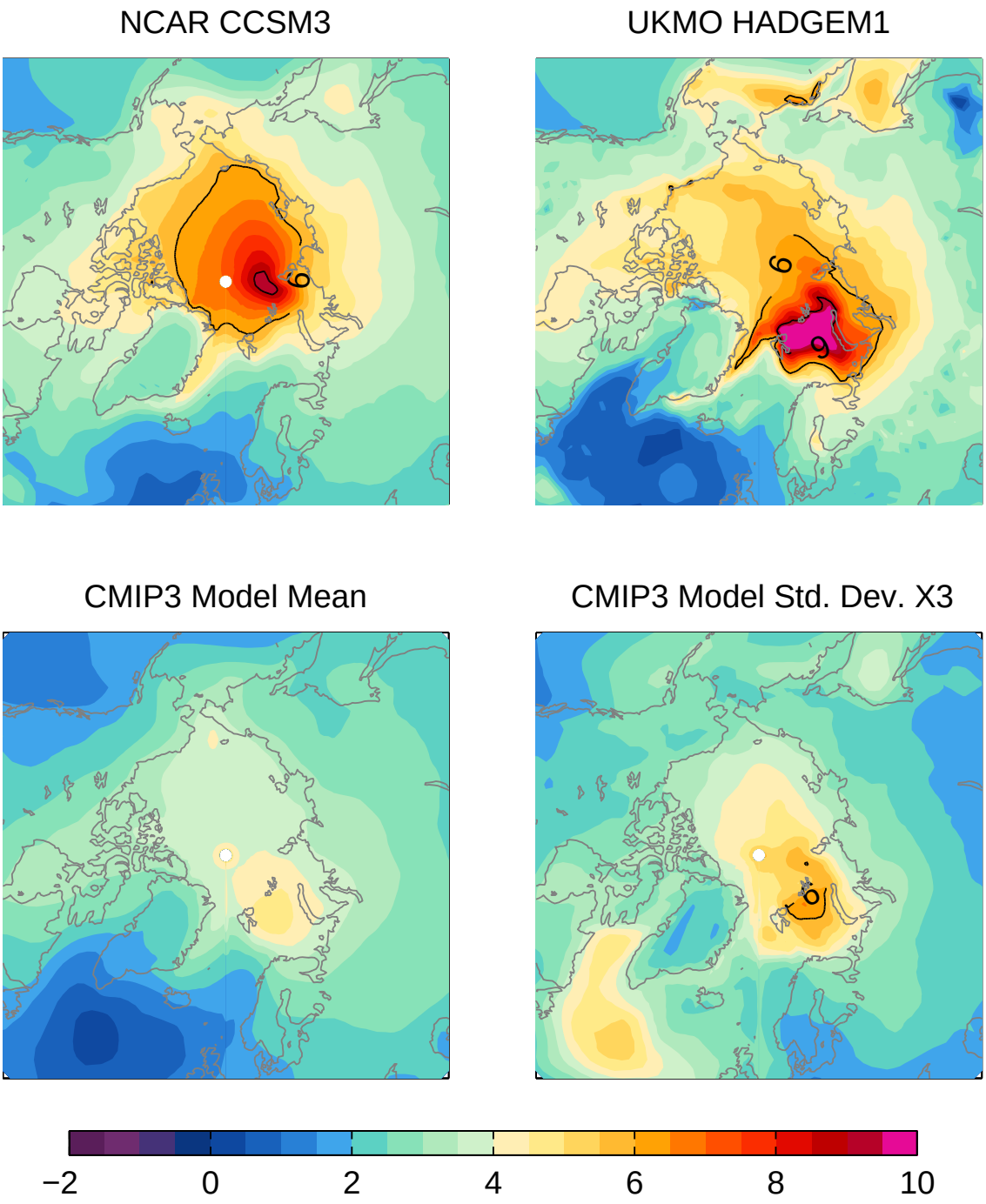

Fig. 6. Change in mean surface air temperature at mid 21st century in °C (2040-2059 minus 1980-1999) (a-c) and across-model standard deviation (d) scaled by a factor of 3.

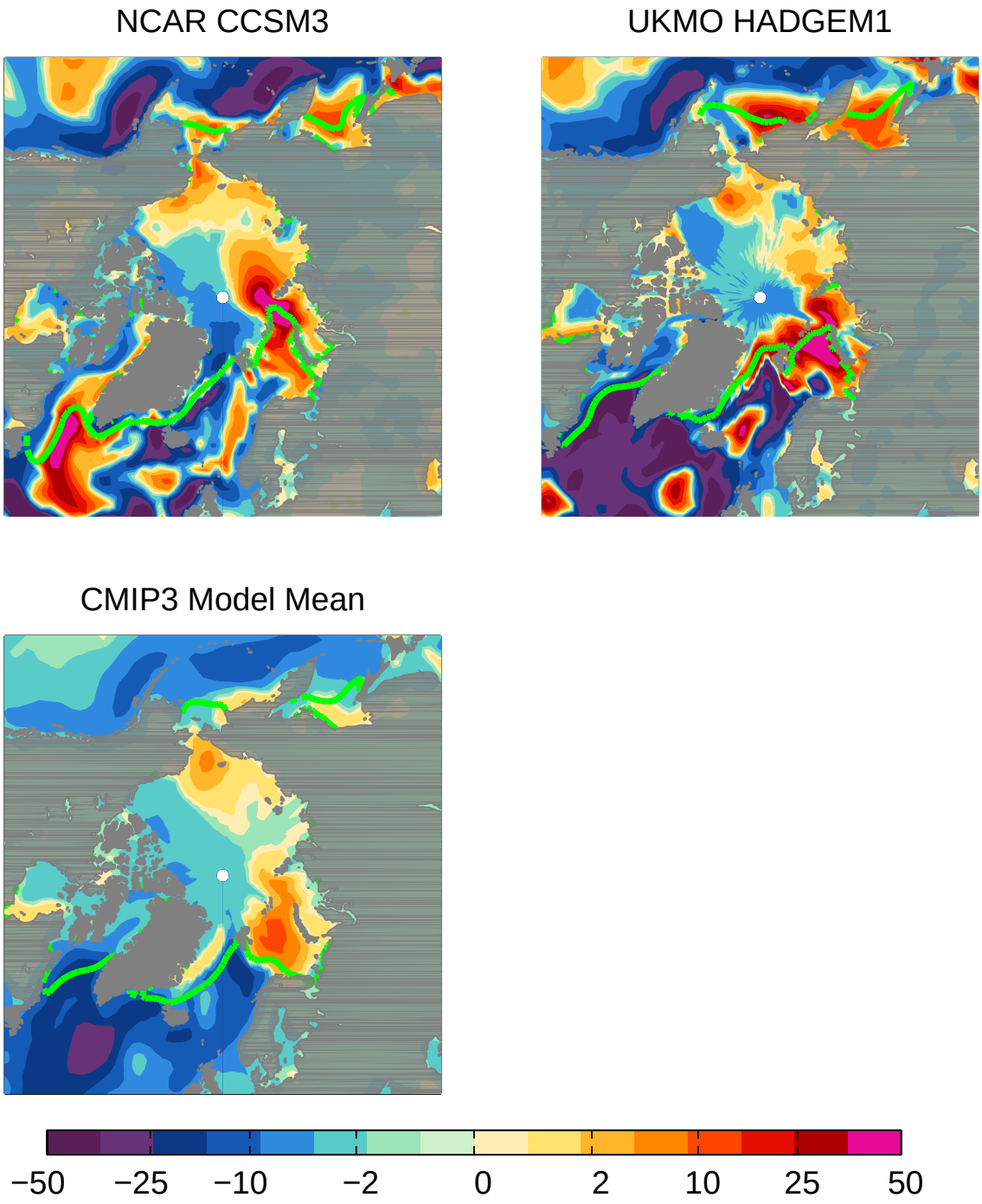

Fig. 7. Change in mean net surface heat flux at mid 21st century in W m^{-2} (2040-2059 minus 1980-1999) with 2040-2059 mean sea ice extent. Positive indicates upwards. Ice extent is defined as the 15% concentration contour.

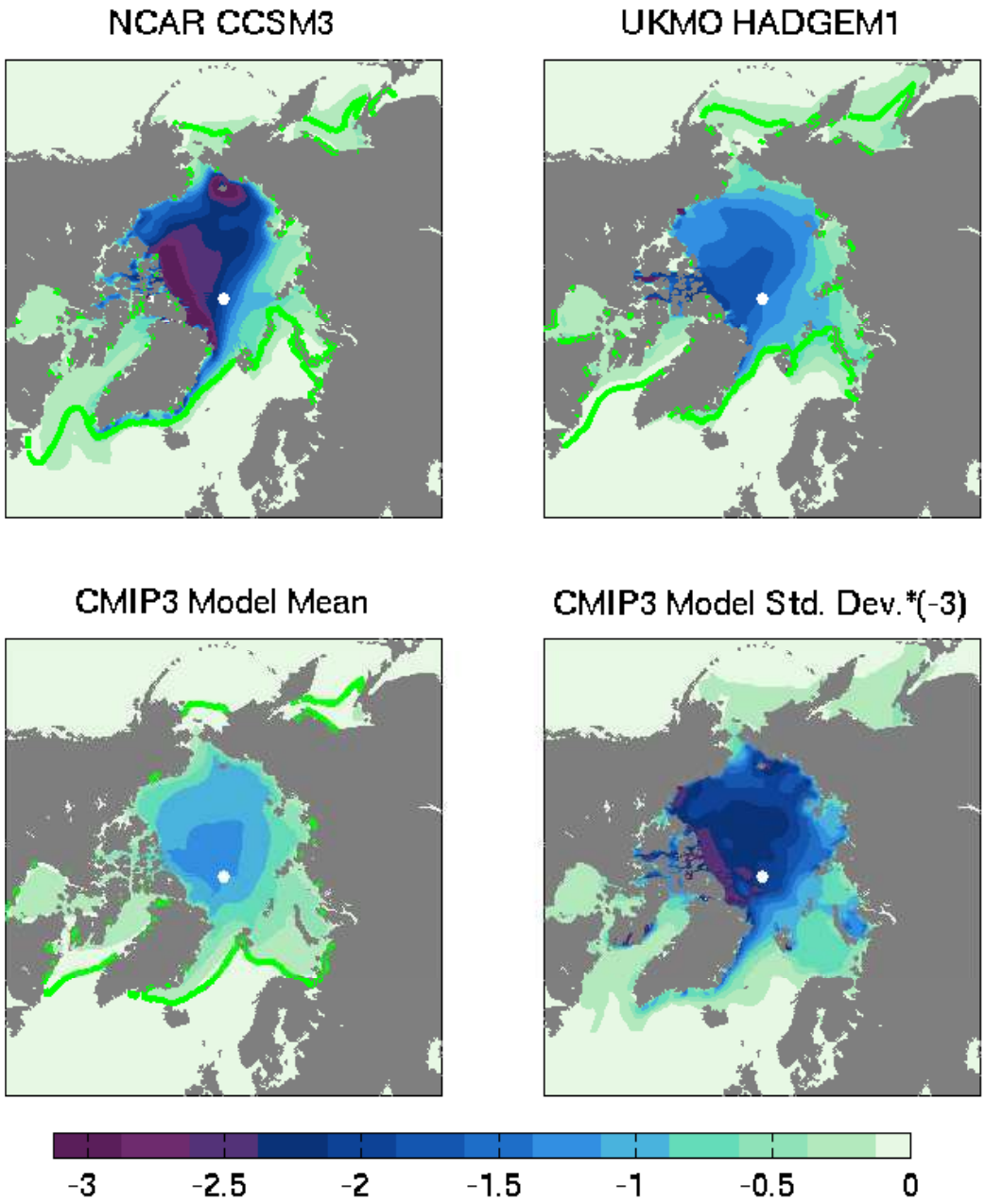

Fig. 8. Change in annual mean sea ice thickness at mid 21st century in m (2040-2059 minus 1980-1999) with the 2040-2059 annual mean ice extent (green line) (a-c) and across-model standard deviation (d) scaled by a factor of -3.

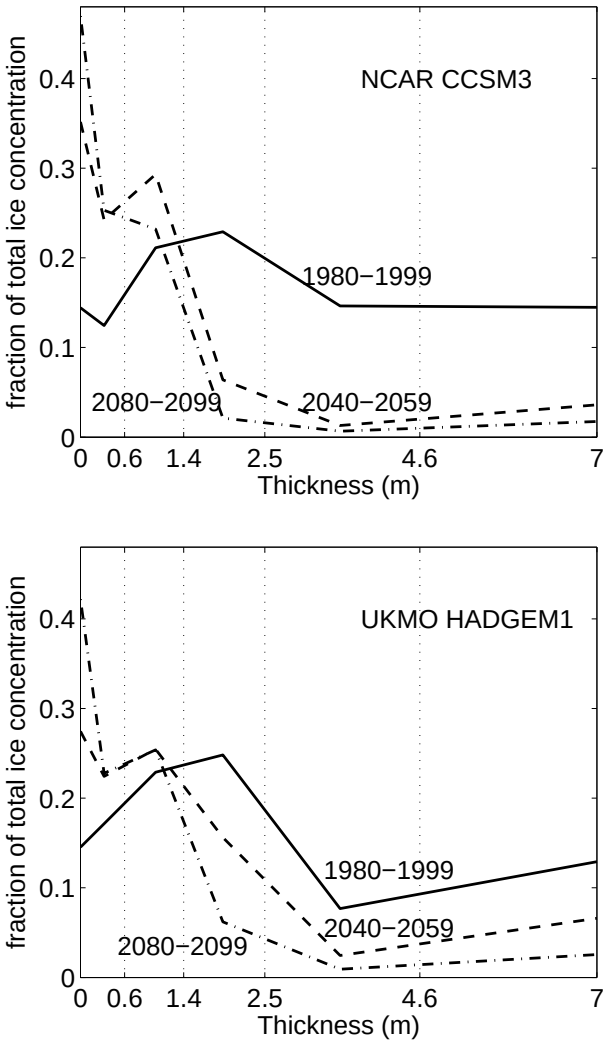

Fig. 9. Annual mean sea ice thickness distribution averaged from 75-90N only where the sea ice concentration is 15% or greater in individual years.

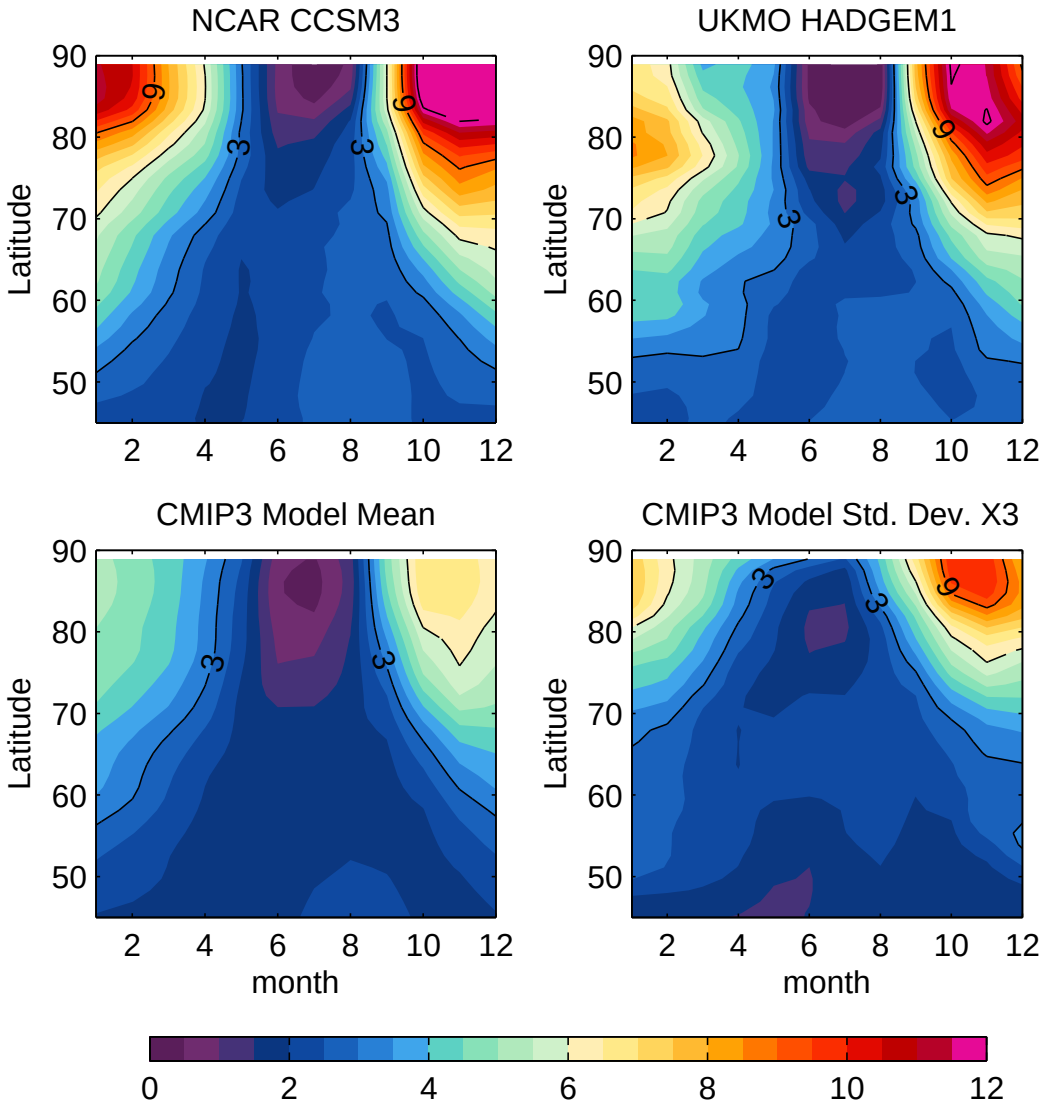

Fig. 10. Change in mean annual cycle of the zonally averaged surface air temperature at mid 21st century in °C (2040-2059 minus 1980-1999) (a-c) and across-model standard deviation (d).

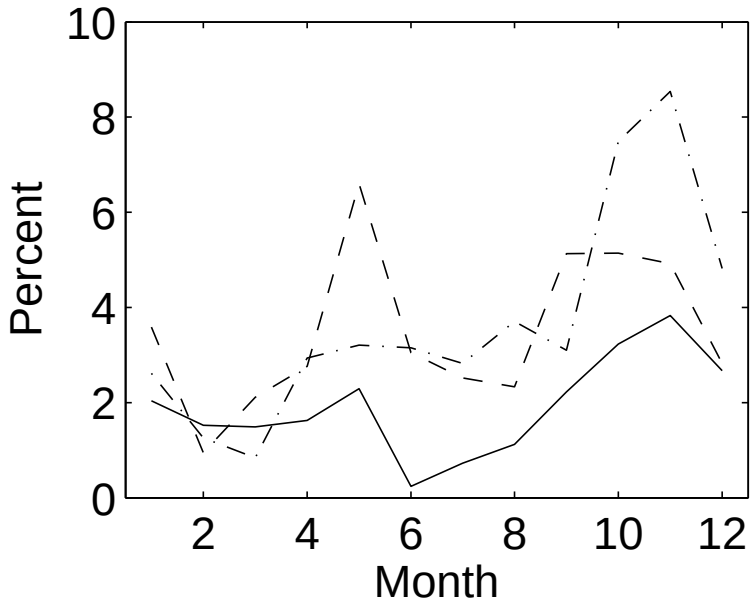

Fig. 11. Change in percent of total cloud cover at mid 21st century (2040-2059 minus 1980-1999) averaged 70-90°N in CCSM3 (dot-dashed), HADGEM1 (dashed), and the CMIP3 Model Mean (solid).

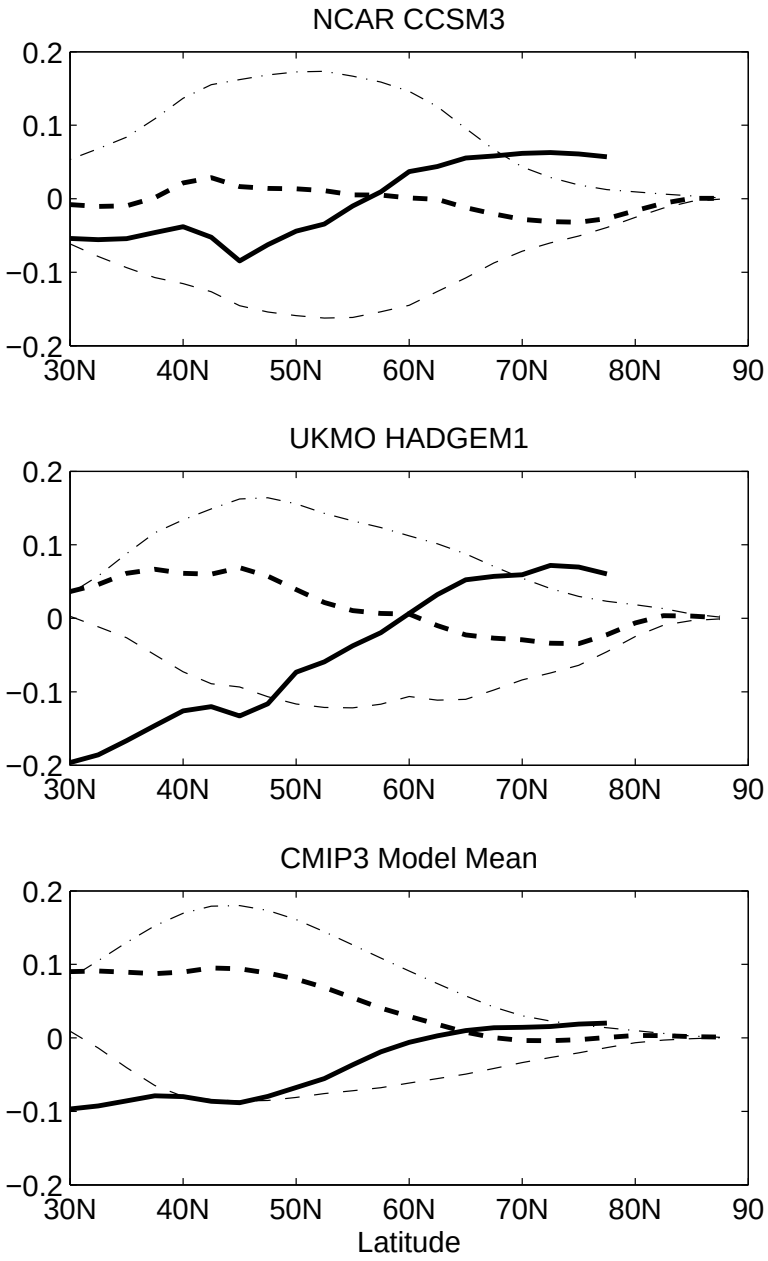

Fig. 12. Change in atmospheric and oceanic heat transport (thick dashed and solid lines, resp.) at mid 21st century in PW (2040-2059 minus 1980-1999). The atmospheric heat transport is broken into latent energy and dry static energy components (thin dot-dashed and dashed, resp.).